Master's Thesis

Design, Build and Test of Planar Antennae

Constantine Ayimba

Department of Electrical and Information Technology,
Faculty of Engineering, LTH, Lund University, 2016.

Department of Electrical and Information Technology

LUND
UNIVERSITY

Design, Build and Test of Planar Antennae

Constantine Ayimba

Supervisor: Doruk Tayli

Examiner: Mats Gustafsson

Submitted in part fulfillment of the requirements for the degree of
Masters in Wireless Communications of Lund University, June 2016

Abstract

Planar antennae have become very popular owing to their relative ease of manufacture and unobtrusive nature (they are conformal to surfaces) especially with regard to certain devices such as smart phones, watches and fitness gadgets. Although the fractional bandwidth of planar antennae is small, the actual bandwidth in absolute terms is high owing to the higher centre frequencies used and proves useful for these applications.

The department of Electrical and Information Technology at Lund University has acquired an LPKF™ ProtoLaser U3 prototyping machine for the purpose of fabricating planar antennae for various research applications. This work reviews the process required to create reliable antennae using this machine and posits important criteria that should be considered.

The Frequency Domain Solver in the Microwave Studio package of the Computer Simulation Toolkit(CST) has been employed in the design and simulation of self resonant antennae at 5.2 GHz, 15 GHz and 28 GHz. The frequency response of the reflection coefficient of a fabricated antenna was found to be in good agreement with simulations if the substrate's dielectric constant and loss tangent was properly modelled in the simulations. The measured responses of fairly intricate designs were found to deviate more from simulations compared to simple designs.

Acknowledgements

I would first and foremost like to thank the Swedish Institute for awarding the scholarship and wherewithal which made it possible for me to pursue this Masters degree. Their contribution is a testament to their commitment to advance progress through empowerment.

I am also greatly indebted to my advisors Doruk Tayli and Mats Gustafsson who transformed every challenge into an opportunity to improve my thinking around unforeseen impediments.

Special thanks to Martin Nilsson and Andreas Johansson for their unyielding help at the outset of the project to provide the resources needed to bring this project to birth.

List of Acronyms

AUT	Antenna Under Test
CAD	Computer Aided Design
CEM	Computational Electromagnetics
CST	Computer Simulation Technology
EurAAP	European Association on Antennas and Propagation
FEM	Finite Element Method
FR4	Flame Retardant 4
PCB	Printed Circuit Board
SMA	SubMiniature version A
TE	Transverse Electric Waves
TM	Transverse Magnetic Waves
VNA	Vector Network Analyser

Table of Contents

Abstract i

Acknowledgements iii

List of Acronyms v

1 Introduction 1

1.1 Background 1

1.2 Problem Statement 4

1.3 Thesis Outline 5

2 Computer Aided Design 7

2.1 Maxwell's Equations 7

2.2 Simulation Considerations 9

2.2.1 Modeling 9

2.2.2 Meshing 9

2.2.3 Material Characterisation 9

2.3 Software Selection 11

2.4 Solvers 12

3 Antenna Design & Manufacturing 13

3.1 Antenna dimensions 13

3.2 Feed types 14

3.2.1 Direct Feed 14

3.2.2 Microstrip Feed 14

3.2.3 Coupled Feeds 16

3.2.4 Connectors 17

3.3 Designs 19

3.3.1 Standard Patch Antenna 20

3.3.2 Slotted Patch Antenna 21

3.4 Design Optimisation 21

3.5 Manufactured specifications 25

3.6 Approximation of effective dielectric constant and loss tangent 25

3.6.1 Estimation of FR4 parameters by antenna prototyping 25

3.6.2 Estimation of Rogers™ substrate parameters using the quarter wave stub 26

3.7 Manufacturing process 28

4 Results 31

4.1 Measurement Setup 31

4.2 5.2 GHz Prototypes 31

4.2.1 Permittivity and loss estimates 31

4.2.2 Relative performance 36

4.3 15 GHz Prototypes 36

4.3.1 Permittivity and loss estimates 36

4.3.2 Antenna performance 37

4.4 28 GHz Prototypes 40

5 Conclusion 43

5.1 Summary 43
5.2 Future Work 44

Bibliography **44**

Appendix **49**

A Optical Microscope Measurements **49**

List of Tables

3.1 5.2 GHz antennae with FR4 Substrate (h=0.8 mm, $\epsilon_{\mathrm{r}} \approx 3.92$ (estimate)) 23

3.2 15 GHz antennae with Rogers™ 3003 Substrate (h=0.5 mm, $\epsilon_{\mathrm{r}} \approx 2.854$ (estimate)) 25

3.3 28 GHz antennae with Rogers™ 3003 Substrate (h=0.5 mm, $\epsilon_{\mathrm{r}} \approx 2.861$ (estimate)) 25

4.1 Approximate % deviation from design for standard antennae at 15 GHz 40

4.2 Approximate % deviation from design for slotted antennae at 15 GHz 40

4.3 Approximate % deviation from design for standard antennae at 28 GHz 40

A.1 Measurements of standard antennae at 15 GHz 49

A.2 Measurements of slotted antennae at 15 GHz 49

A.3 Measurements of standard antennae at 28 GHz 50

List of Figures

1.1 Circuit schematic of transmit and receive antennae 2
1.2 Reflection coefficient and antenna bandwidth 3

2.1 Tetrahedron mesh of a patch and SMA feed 10

3.1 Standard rectangular patch with SMA feed 15
3.2 Microstrip feed line design parameters 16
3.3 Slot coupled stripline feed 17
3.4 SMA end launch connector 18
3.5 SouthWest Microwave™ end-launch connector 18
3.6 Detail of PCB for use with SouthWest Microwave™ end-launch connector 19
3.7 Standard patch with microstrip line feed 20
3.8 Slotted patch with SMA feed 21
3.9 Slotted patch with microstrip feed 22
3.10 S-parameters of the antenna depicted in a Smith Chart. The optimisation goal definition is shown as the black arrow. . . . 24
3.11 Quarter wave stub resonator 27
3.12 LPKF™ ProtoLaser U3 machine 29

3.13 Protective screen detail 29
3.14 Machining detail (a) Diagonal cut (b) Grid cut 30

4.1 Measurement Setup 32
4.2 FR4 antenna prototype return loss. For simulations the relative permittivity was estimated at $\epsilon_{\mathrm{r}} = 4.3$ and the connector is modeled as a transmission line of length 2.4mm 32
4.3 FR4 antenna prototype return loss. For simulations the relative permittivity was estimated at $\epsilon_{\mathrm{r}} = 4.3$ and the connector is modeled as a transmission line of length 8.0mm 33
4.4 FR4 antenna prototype impedance response. For simulations the relative permittivity was estimated at $\epsilon_{\mathrm{r}} = 4.3$ and the connector is modeled as a transmission line of length 2.4mm . 33
4.5 FR4 antenna prototype impedance response. For simulations the relative permittivity was estimated at $\epsilon_{\mathrm{r}} = 4.3$ and the connector is modeled as a transmission line of length 8.0mm . 34
4.6 Comparison of return loss. For simulations the relative permittivity was estimated at $\epsilon_{\mathrm{r}} = 3.92$ F.L.=Feed Length, $\tan\delta$=loss tangent 35
4.7 Comparison of resistance values about resonance A (F.L.=2.4mm, $\tan\delta$=0.025), B (F.L.=8.0mm, $\tan\delta$=0.025), C (F.L.=8.0mm, $\tan\delta$=0.015), M (Measurement) 35
4.8 Comparison of reactance values about resonance A (F.L.=2.4mm, $\tan\delta$=0.025), B (F.L.=8.0mm, $\tan\delta$=0.025), C (F.L.=8.0mm, $\tan\delta$=0.015), M (Measurement) 36
4.9 Comparative Return loss performance 37
4.10 Insertion loss characteristic of quarter wave stub 38
4.11 Relative permittivity estimate of Rogers™ 3003 substrate . . . 38

4.12 Return loss response of standard antennae 39
4.13 Return loss response of slotted antennae 39
4.14 Comparison of Standard and Slotted antenna responses 41
4.15 Return loss response of the standard antenna 41
4.16 Comparison of antenna responses. Simulation with higher loss tangent. 42

A.1 Vectorised images for measurement of antennae 50
A.2 Comparative reference measurement 51

Chapter 1

Introduction

1.1 Background

A brief overview of some important antenna characteristics is presented in this chapter.

At the heart of every wireless communication system is the antenna. It is essentially a device that converts a guided electromagnetic wave on a transmission line to a propagating wave in free space and vice-versa [1].

The ability of an antenna to effectively transmit and receive electromagnetic waves (the means through which wireless communication takes place) depends on its efficiency which in turn depends in large part on its design and the properties of the dielectric material used e.g. permittivity, loss tangent, conductivity and dispersion characteristics.

An important consideration is how well the antenna is matched to the transmission line which determines how much of the power delivered to the antenna. The reflection coefficient (Γ) is a figure of merit indicating how much power is reflected back to the input owing to the disparity in matching. The lower the value of (Γ), the higher the value of accepted power at the antenna input as depicted in Fig 1.1. This is calculated as [1]:

$$\Gamma = \frac{Z_{\mathrm{A}} - Z_0}{Z_{\mathrm{A}} + Z_0}, \tag{1.1}$$

where Z_{A} is the antenna input impedance and Z_0 is the characteristic

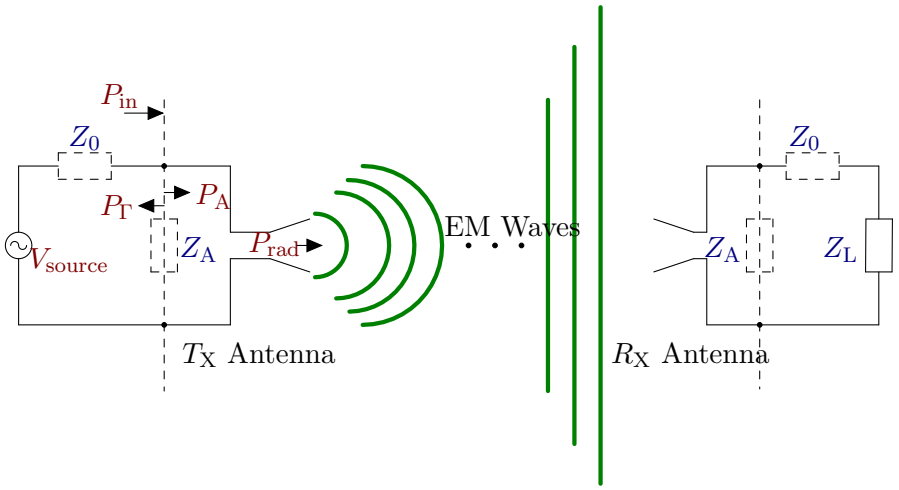

Figure 1.1: Circuit schematic of transmit and receive antennae

impedance of the transmission line (for many applications is real valued at 50 Ohm). The power accepted at the antenna input, P_{A}, as a function of the reflection coefficient is calculated as [1]:

$$P_{\text{A}} = (1 - |\Gamma|^2)P_{\text{in}}, \tag{1.2}$$

where P_{in} is the input power.

Inherent inductance and capacitance also leads to some energy storage within the antenna. The quality factor (Q) gives an indication of how much energy oscillates between the magnetic and electric field and is defined as[2]

$$Q = \eta_{\text{eff}} \frac{2c_0 k \max\{W_{\text{m}}, W_{\text{e}}\}}{P_{\text{rad}}}, \tag{1.3}$$

where $\eta_{\text{eff}} = (P_{\text{rad}}/P_{\text{A}})$ is the antenna efficiency with P_{A} as the power accepted at the antenna, P_{rad} is the radiated power, c_0 is the speed of light, k is the free space wave number, W_{m} is the stored magnetic energy and W_{e} is the stored electric energy.

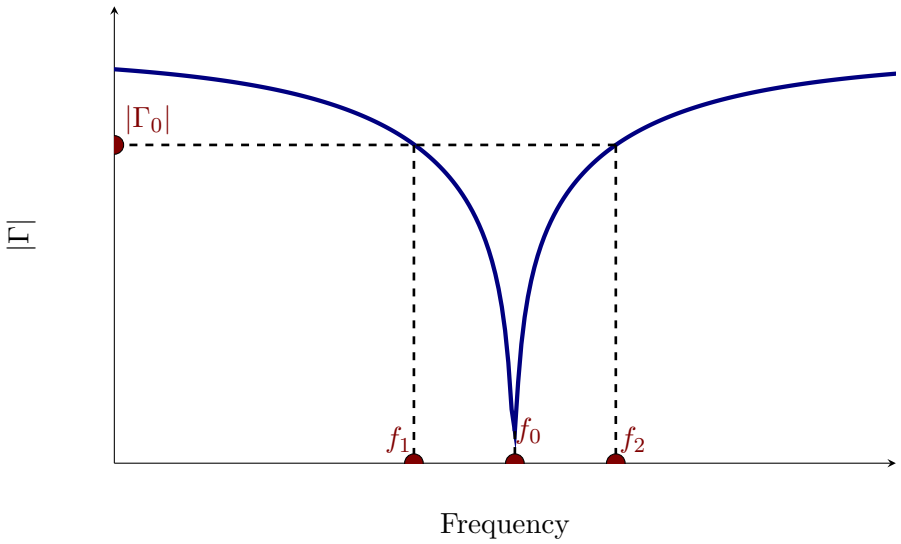

Figure 1.2: Reflection coefficient and antenna bandwidth

The range of frequencies over which the antenna conforms to a given characteristic, for instance the reflected power around the resonant frequency being below a given threshold, is called the bandwidth of the antenna[1].

The fractional bandwidth of an antenna can be defined as:

$$B = \frac{f_2 - f_1}{f_0}, \tag{1.4}$$

where f_0 is the resonant frequency, f_1 and f_2 are the lower and upper frequency bounds respectively satisfying maximum allowable reflection coefficient (e.g. $\Gamma_0 \approx 0.3$ equivalent to -10 dB reflected power). This is depicted in Figure 1.2.

For typical narrowband planar antennae, an approximate fractional bandwidth value is related to the magnitude of the reflection coefficient at resonance by[2]

$$B \approx \frac{2}{Q} \frac{|\Gamma_0|}{\sqrt{1 - |\Gamma_0|^2}}, \text{ for } Q \gg 1, \tag{1.5}$$

where B is the fractional bandwidth, Γ_0 is the maximum tolerable reflection coefficient and Q is the quality factor, see Figure 1.2.

As is evident from equation (1.5) the larger the value of Q the smaller the fractional bandwidth for a given reflection coefficient. Typical values of fractional bandwidth for planar antennae are about six to ten per cent depending on the substrate thickness [3].

For planar antennae, design strategies are geared at keeping the Q factor low by a proper selection of dielectric material, its thickness as well as the overall radiating structure and feed network.

Thin substrates are used in many applications of planar antennae particularly at high frequencies resulting in low fractional bandwidths, however the absolute bandwidth obtainable at such high frequencies can be quite large (5% of $5\,\mathrm{GHz} = 250\,\mathrm{MHz}$).

1.2 Problem Statement

Planar antennae are preferred in many modern day applications such as smart phones, smart watches, as well as proposed designs for the internet of things as they are unobtrusive, easy to manufacture and incorporate into the integrated circuitry of these devices [4].

The pre-eminence of planar antennae in these applications make their study important as communication systems transition to ever higher frequencies. To this end, among others, the department of Electrical and Information Technology at Lund University has acquired a precision laser prototyping machine to manufacture planar antennae for a host of research projects.

The purpose of this work is to explore how best to align the design and manufacturing process to produce antennae. In this work, antennae for use at $5\,\mathrm{GHz}$, $15\,\mathrm{GHz}$ and $28\,\mathrm{GHz}$ range of frequencies are designed and fabricated.

The design process is primarily carried out using the Microwave Studio package available in the Computer Simulation Toolkit (CST) suite as well as data modelling tools in MATLAB.

1.3 Thesis Outline

Chapter 2 presents a brief review of computational design tools owing to their increasing prominence in antennae design. Chapter 3 outlines the chosen designs detailing aspects of their structure that can be adjusted to procure the desired response at a given frequency. Chapter 4 presents and compares the results obtained from the simulation tools prior to manufacture and those obtained from actual measurements of the manufactured antennae. Chapter 5 draws conclusions and makes recommendations for future prototyping using the laser tool.

Chapter 2

Computer Aided Design

Mathematical modeling techniques such as the transmission line and modal expansion cavity model [3] for analysing planar antenna may prove too onerous if the antenna has an intricate design. In such cases it is expedient to analyse the antenna using numerical techniques implemented in software as solutions to Maxwell's equations of electromagnetic theory.

In recent years, numerical techniques have become standard fare in the design of radiating structures with the advent of software tools whose results closely mirror actual measured results [5].

2.1 Maxwell's Equations

Maxwell's equations are a set of equations formulated by James Clark Maxwell [6] as a way of unifying fundamental deductions obtained from experiments in electromagnetics carried out by Gauss, Faraday and Ampère among others. They were further expressed using elegant vector notation by Heaviside into their present form presented in equations (2.1) to (2.4).

Gauss' law describes the behaviour of the Electric field in the vicinity of electric charges. When expressed as an integral, it points to the observation that the sum of the electric flux emanating from a given enclosed space (volume) is equal to the total electric charge within it. The vector form of this law is stated as:

$$\nabla \cdot \mathbf{D} = \rho_{\mathrm{v}} \tag{2.1}$$

where $\mathbf{D}$ ($\mathrm{C/m^2}$) is the electric flux density and ρ_v ($\mathrm{C/m^3}$) is the volume charge density.

Gauss' law for magnetism asserts that there can be no free magnetic charges (monopoles). Empirically magnets exist as dipoles, and as such magnetic fields flowing out of an enclosed surface are equal to those flowing into it. There is no net flow of magnetic flux into or out of a volume. This can be expressed as:

$$\nabla \cdot \mathbf{B} = 0 \tag{2.2}$$

where $\mathbf{B}$ ($\mathrm{Wb/m^2}$) is the magnetic flux density.

Faraday's law states that a time varying magnetic field induces an electric field. This can be stated as:

$$\nabla \times \mathbf{E} = -\frac{\partial \mathbf{B}}{\partial t} \tag{2.3}$$

where $\mathbf{B}$ ($\mathrm{Wb/m^2}$) is the magnetic flux density and $\mathbf{E}$ (V/m) is the electric field strength.

Ampere's law states that a time varying electric field gives rise to a magnetic field. In vector form this can be expressed as:

$$\nabla \times \mathbf{H} = \frac{\partial \mathbf{D}}{\partial t} + \mathbf{J} \tag{2.4}$$

where $\mathbf{H}$ (Wb/A) is the magnetic field strength, $\mathbf{E}$ (V/m) is the electric field strength and $\mathbf{J}(\mathrm{A/m^2})$ is the current density.

The equations (2.1) to (2.4) when applied to an antenna structure with constraints on boundary conditions can be used to calculate surface currents as well as predict the behaviour of the electric and magnetic fields of the antenna. Antenna properties such as reflected power, radiation efficiency etc. can thus be calculated. This is what is done in computational electromagnetics and is the basis of antenna design software [7].

2.2 Simulation Considerations

2.2.1 Modeling

In this work, it has been observed that to obtain reliable simulation results the physical model of the antenna should be as similar as possible to the actual antenna. Whereas it is possible to simplify physical models to reduce computational complexity, in some cases what appears trivial in the design e.g. the feed structure may alter the simulation results and create significant disparities with actual measurement data [8].

2.2.2 Meshing

In order to apply numerical techniques, the solutions to Maxwell's equations can be discretised by dividing up a structure into small regions, imposing boundary conditions and solving the resulting system of equations. This is known as meshing.

For some solvers such as the Finite Element Method (FEM) solver, increasing the density of the mesh particularly along the edges of the object improves the accuracy of the simulation. This is so because the current density is higher along the edges [9].

Depending on the solver employed, the structure can be divided up into polygons of different shapes in such a way as to both accurately describe the physical structure as well as facilitate the quick solution of Maxwell's equations.

2.2.3 Material Characterisation

A crucial consideration in modeling an antenna for simulations is the accurate characterisation of its properties such as: conductivity, permeability, permittivity as well as its losses. Such losses are the result of friction and consequent energy dissipation in the form of heat as the dipoles align and re-align in response to a time-varying electric field. In many instances it is common to model these losses as a loss tangent. Permittivity (ϵ) in this case is expressed as a complex quantity to model the phase shift between

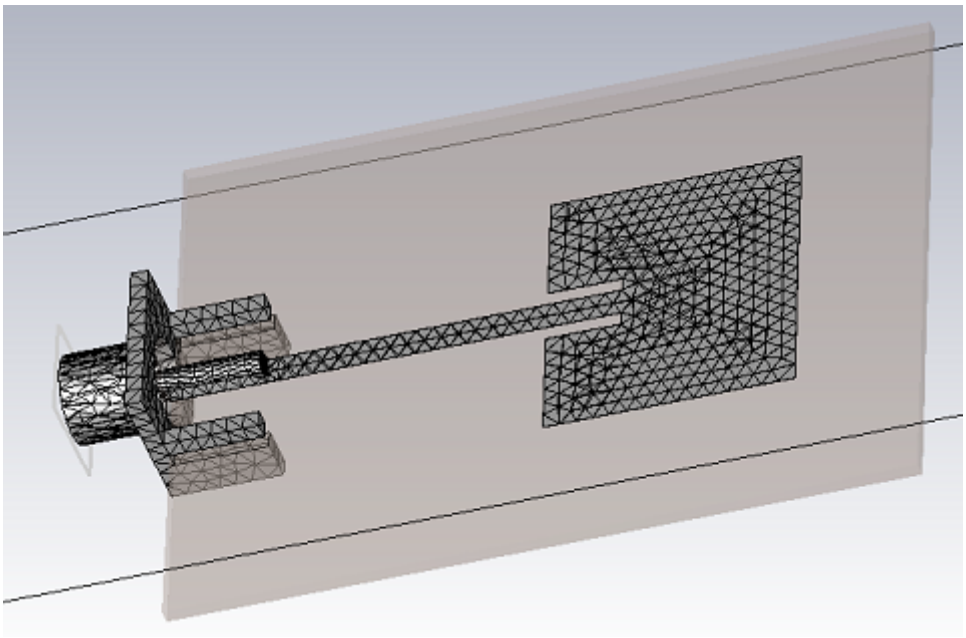

Figure 2.1: Tetrahedron mesh of a patch and SMA feed

the electric flux density and the electric field [1]:

$$\mathbf{D} = \epsilon \mathbf{E}, \tag{2.5}$$

$$\epsilon = \epsilon' - \mathrm{j}\epsilon''. \tag{2.6}$$

An equivalent means of characterising the dielectric loss is by modelling it as conductivity in the material, in which case the displacement current **J** can be espressed as [1]

$$\mathbf{J} = \sigma \mathbf{E}. \tag{2.7}$$

Equation (2.4) then becomes [1]

$$\nabla \times \mathbf{H} = \mathrm{j}\omega\{\epsilon' - \mathrm{j}(\epsilon'' + \frac{\sigma}{\omega})\}\mathbf{E}. \tag{2.8}$$

It should be noted that some authours e.g. Bladel [10], directly include the σ/ω term in the ϵ'' term of equation (2.6).

From equation 2.8, the loss tangent can then be defined as [1]

$$\tan\delta = \frac{\omega\epsilon'' + \sigma}{\omega\epsilon'}, \tag{2.9}$$

where δ is the phase difference between the electric flux density $\mathbf{D}$ and the electric field $\mathbf{E}$. At high frequencies the conductivity term is very small compared to the permitivitty terms ($\sigma \approx 0$) [11]:

$$\tan\delta \approx \frac{\epsilon''}{\epsilon'}. \tag{2.10}$$

Dispersion, the shift in the complex permittivity of a material with frequency is marginal over the small range of frequencies typical for narrowband antennae. In the case of broadband antennae, dispersion may need to be modelled correctly to compensate for the change in loss characteristics as the frequency varies. The Debye [12] or Lorentz [13] model can be used in simulations to account for this frequency dependence. In this instance both the real and imaginary parts of the permittivity are functions of frequency as shown in equation (2.11),

$$\epsilon = \epsilon'(\omega) - \mathrm{j}\epsilon''(\omega). \tag{2.11}$$

The mutability of a material when subjected to electromagnetic energy largely accounts for observed differences between measured and simulated values (when the measurement environment such as objects around the near field are properly controlled for). At microwave frequencies losses in the dielectric are more pronounced than those of the metal of a planar structure [11], in such cases therefore it is enough to characterize the loss in the substrate and not those of the conductor.

2.3 Software Selection

The EurAAP has been actively involved in coordinating the work of antenna researchers and commercial antenna software companies to unify

their efforts in order to create better design tools [8]. Commercial software as opposed to custom built in-house tools are most commonly used in antenna design [8]. It is therefore crucial to have common baselines so that the results obtained from these tools can be reliable for design purposes. Even though the use of software for antenna design has gained traction over many years, simulation results obtained from using different tools in recent times still show significant differences [8].

The choice of the software tool to use depends to a large extent on its availability. A number of such software were deemed too expensive at the EurAAP conference mentioned in [8]. EIT has licenses for significant features of CST Microwave Studio making it a convenient choice for antenna modeling and design. It is also widely used among the research community [8].

2.4 Solvers

The broad classification of solvers places them into two categories, those that solve Maxwell's equations in integral form and those that solve them in differential form [9]. Integral solvers include the Method of Moments (MoM), differential solvers can be further divided into Finite Element Method (FEM) and Finite Differences in Time Domain solvers (FDTD).

The choice of solver is determined by factors such as the complexity of the structure, the nature of the substrate (homogeneity, isotropic/non-isotropic) and simulation time constraint among others. For instance whereas integral equation solvers are very efficient for simple structures with homogeneous media, differential solvers such as the FEM can better simulate structures that are more complex (with finer details) and whose constitution may include inhomogeneous media such as different substrates [9].

Ideally all solvers should converge to similar results given that they are different approaches to solving Maxwell's equations but this in many instances is not the case as mentioned in [9]. FEM was chosen for this work owing primarily to its versatility in dealing with intricate structures.

Chapter 3

Antenna Design & Manufacturing

3.1 Antenna dimensions

In this section extensive reference is made to Figure 3.1. The dominant TM_{10} mode of operation for which the patch antenna radiates upwards from the ground plane can be excited by adjusting the length (L) of the radiating edges to be approximately half a wavelength (in the substrate) at the resonant frequency [3]:

$$L \approx \frac{1}{2}\frac{\lambda_0}{\sqrt{\epsilon_\mathrm{r}}}, \tag{3.1}$$

where ϵ_r is the nominal relative permittivity defined as $\epsilon_\mathrm{r} = (\epsilon/\epsilon_0)$ and ϵ_0 is the permittivity of free space. From Figure 3.1, the size (W) of the non-radiating edges need to be made larger than the length (L) such that:

$$\frac{W}{L} < 2. \tag{3.2}$$

The condition as expressed in equation (3.2) is necessary to avoid the resulting efficiency from becoming too low [3].

A further important consideration is the radiation resistance at resonance which is a strong function of the feed position. If the antenna is modeled as a resonant cavity formed by the patch and the ground plane as perfectly conducting electrical boundaries and the dielectric faces as perfect magnetic boundaries, the strength of the electric field is determined to be strongest at the two radiating edges of the patch [3].

In order to attain good matching at resonance (hence reduce reflected power as mentioned in Section 1.1) it is common practice to offset the feed slightly from the non-radiating edge so that the resulting radiation resistance is as close as possible to the characteristic impedance of the transmission line. The radiation resistance at this offset distance can be approximated by [3]:

$$R_{\text{rad}} \approx R_{\text{edge}} \cos^2\left(\frac{\pi x}{L}\right) \tag{3.3}$$

where R_{edge} is the radiation resistance at the edge of the patch, x is the offset from the edge and L is the length of the patch as shown in Figure 3.1.

For a given fixed offset (x) from a radiating edge, the field strength for a homogeneous cavity is uniform laterally with the effect that the feed can be located at any location along (W) in Figure 3.1 without changing the impedance response. For many applications it is common to position the feed at the midpoint i.e. ($W/2$) to obtain a uniform polarisation by an even distribution of surface currents on the antenna.

Typically an increase in the width (W) of the patch also has the effect of reducing the radiation resistance at resonance [3].

3.2 Feed types

3.2.1 Direct Feed

A simple way to connect a planar antenna to the underlying circuitry of a radio receiver or transmitter is to make use of a co-axial feed line. The antenna is excited from the ground plane by ensuring that the inner conductor makes contact with the antenna while the outer conductor connects to the ground plane as shown in Figure 3.1. Sufficient metal around the ground plane should be etched off so as to prevent the inner conductor from inadvertently creating a short circuit between the ground plane and the patch antenna.

3.2.2 Microstrip Feed

The more conventional mechanism of exciting a patch antenna is to make use of a microstrip designed to act as a transmission line matched to a characteristic impedance at the desired resonant frequency.

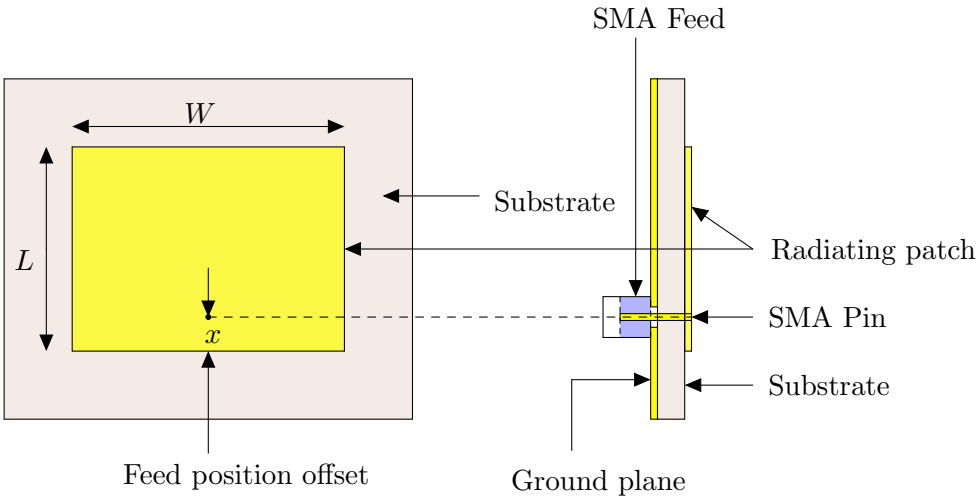

Figure 3.1: Standard rectangular patch with SMA feed

The design of the microstrip feed line is therefore very stringent given the matching requirement. Several techniques have been developed over the years to achieve this as presented by Pozar in [1].

A key consideration is that the electromagnetic wave in a microstrip line is only quasi TEM given that part of it travels in the dielectric material and part through free space [1]. Empirical and numerical techniques attempt to create an effective dielectric constant that takes this fact into account. This can be approximated as [1]:

$$\epsilon_{\text{eff}} = \frac{\epsilon_{\text{r}} + 1}{2} + \frac{\epsilon_{\text{r}} - 1}{2} \frac{1}{\sqrt{1 + 12h/W}}, \tag{3.4}$$

where h is the thickness of the substrate.

The rigorous treatment required to generate the optimal width and length of the microstrip transmission line is beyond the scope of this work but can be found in [14]. Calculations are done using empirical formulae [14].

An example of a typical curve fitting solution to obtain the width of a

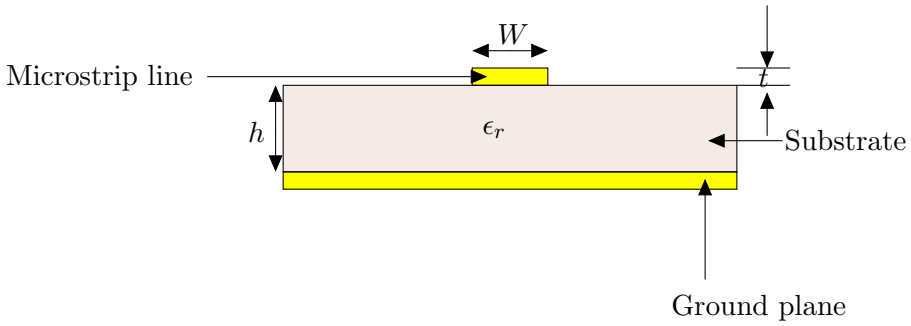

Figure 3.2: Microstrip feed line design parameters

microstrip line needed to match the characteristic impedance is given as [1]:

$$\frac{W}{h} = \begin{cases} 8e^{A}/(e^{2A}-2) & \frac{W}{h} < 2 \\ \frac{2}{\pi}\left[B-1-\ln(2B-1)+\frac{\epsilon_r-1}{2\epsilon_r}\left\{\ln(B-1)+0.39-\frac{0.61}{\epsilon_r}\right\}\right] & \frac{W}{h} > 2 \end{cases} \tag{3.5}$$

where

$$A = \frac{Z_0}{60}\sqrt{\frac{\epsilon_r+1}{2}} + \frac{\epsilon_r-1}{\epsilon_r+1}\left(0.23+\frac{0.11}{\epsilon_r}\right) \tag{3.6}$$

and (3.7)

$$B = \frac{377\pi}{2Z_0\sqrt{\epsilon_r}}. \tag{3.8}$$

Several online applications such as [15] are readily available that carry out these calculations to determine the required widths of microstrip lines once the dielectric substrate, and the thickness of the conductor on the Printed Circuit Board(PCB) is known.

3.2.3 Coupled Feeds

Whenever two unshielded transmission lines are in close proximity, the interaction of their electromagnetic fields results in power coupling between them [1]. This phenomenon can be exploited to deliver excitation to a patch antenna bereft of direct contact between the patch and the transmission

line. Figure 3.3 illustrates this method. Coupled feeds are susceptible to radiation losses owing to the presence of gaps between the feed and the antenna [16].

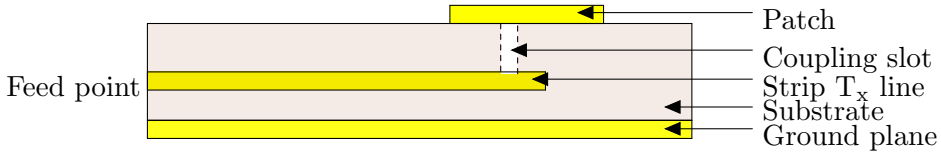

Figure 3.3: Slot coupled stripline feed

3.2.4 Connectors

In order to excite the antenna under test (AUT) from a matched source, the connector used must be fit for purpose. For instance the connector used for the feed mechanism mentioned in 3.2.1 is an SMA Female connector as shown in Figure 3.1. This connector is soldered onto the antenna in such a way as to ensure an electrical connection between the inner conductor and the patch on the one hand and the outer conductor with the ground plane on the other.

For an AUT comprising a microstrip feed-line, two kinds of end-launch connectors were employed such that the microstrip line was fed by the inner conductor and the ground plane had an electrical connection to the outer conductor. The first of these was an SMA connector with supports as shown in Figure 3.4. This required soldering to ensure mechanical support.

The second type of connector used was a special screwable connector from the SouthWest Microwave^{TM} company [17] as shown in Figure 3.5. This particular connector is not soldered to the antenna and could be detached and re-attached to another antenna.

An important consideration when using this connector is that tapering at the edge where the pin makes contact with the microstrip line may be required. The principal reason for this is that the width of the microstrip line, for a particular design frequency, may be too large to fit within the connector pin tunnel and could cause a short circuit with the connector body if left unchanged as shown in Figure 3.6

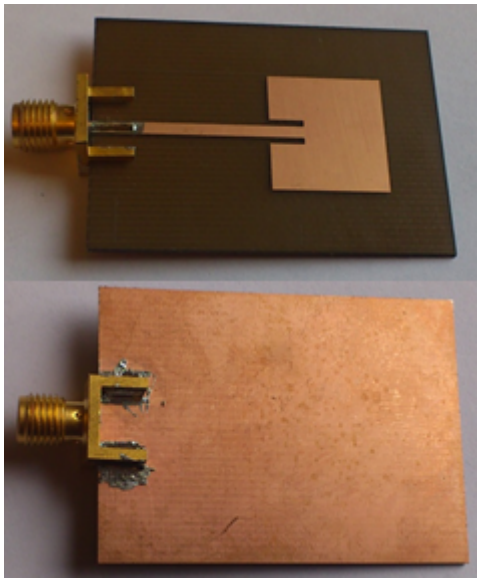

Figure 3.4: SMA end launch connector

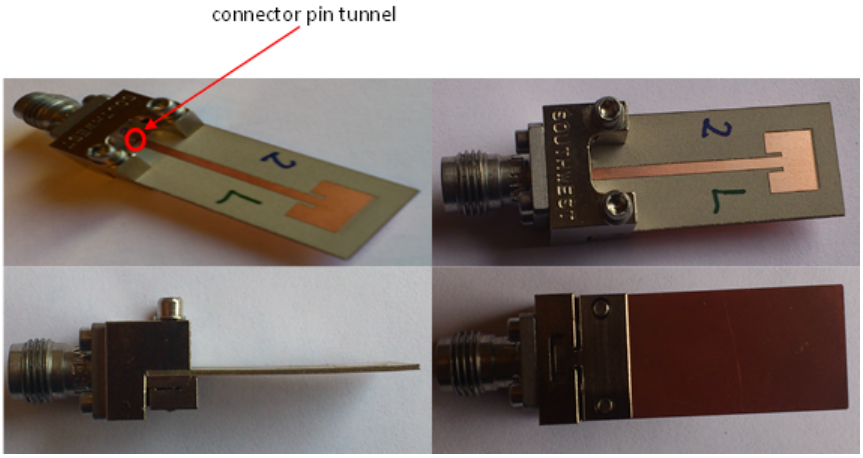

Figure 3.5: SouthWest Microwave™ end-launch connector

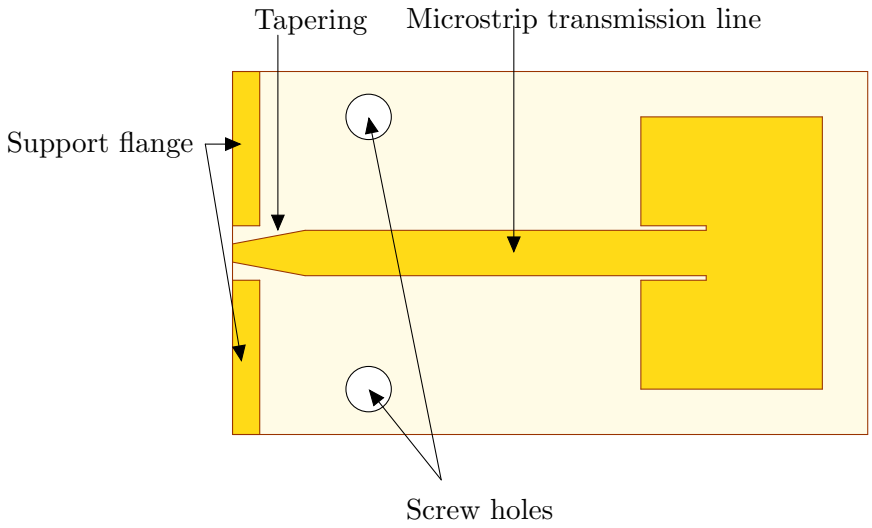

Figure 3.6: Detail of PCB for use with SouthWest Microwave™ end-launch connector

Tapering also improves the performance of the transmission line by adding inductance at the edge of the microstrip transmission line to compensate for the capacitance created at the region of contact between the pin and the microstrip [18].

The optimal tapering to be carried out on the transmission line can be undertaken as an optimisation problem with an aim to minimise insertion loss (S_{21}) of the transmission line considered as a two port system.

3.3 Designs

Two basic designs have been investigated, a standard rectangular patch and a slotted patch. At the lower frequency bounds ($\sim$5 GHz) excitation was effected via both a direct SMA connector and microstrip feed line. In this way both the effect of having slots on the patch and the feed mechanism could be investigated.

At higher frequencies the microstrip feed line is preferred given that the physical size of a direct SMA connector could be in the order of wavelengths and thus impede the response of the standard patch antenna.

3.3.1 Standard Patch Antenna

Figure 3.1 shows the standard patch antenna with the parameters that can be tuned to attain good matching characteristics at resonance. Typically the length (L) has a strong influence on the antenna's resonant frequency. The feed position (x) influences the value of the impedance of the antenna. At resonance (when the impedance is real valued) this should be as close to 50 Ohm as possible so that the return loss is minimised.

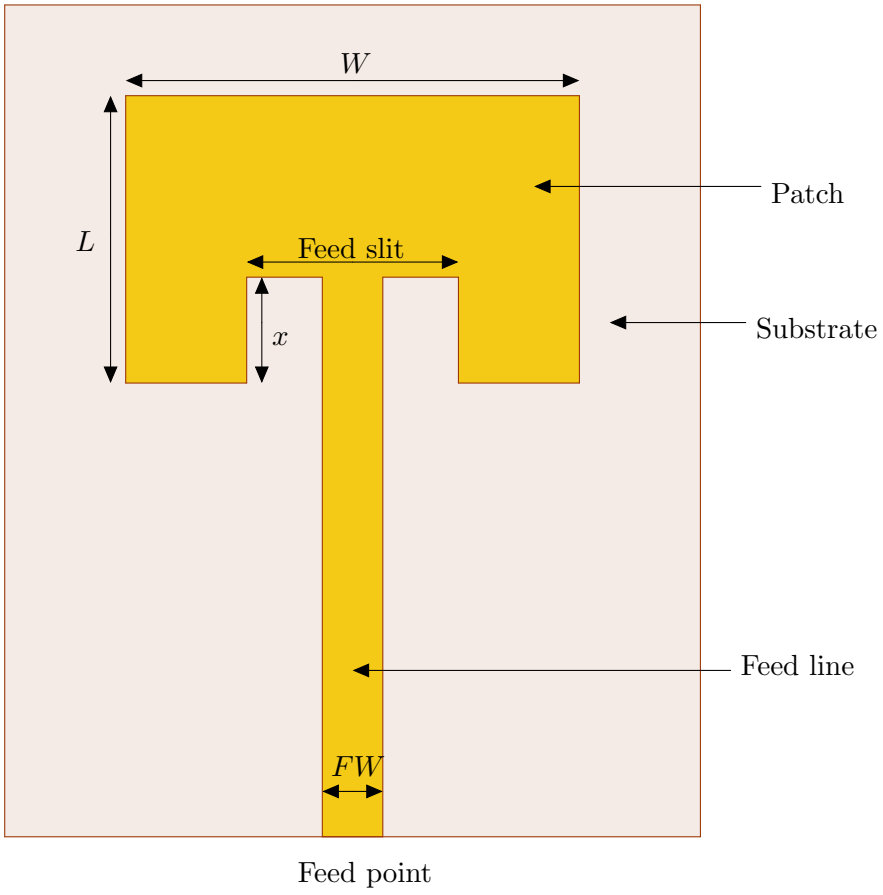

Figure 3.7: Standard patch with microstrip line feed

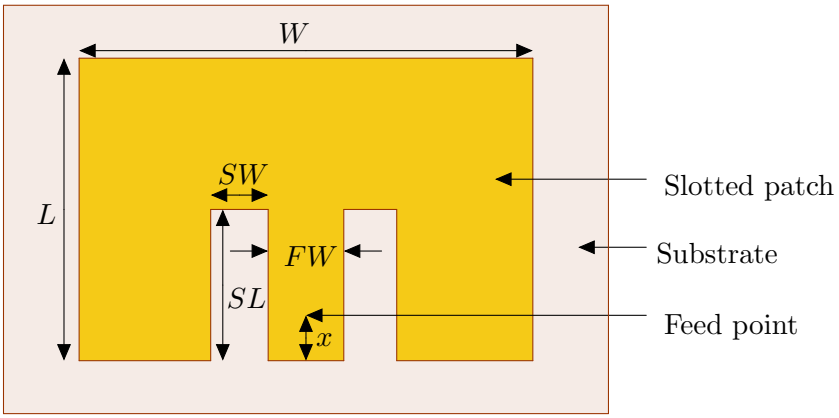

Figure 3.8: Slotted patch with SMA feed

3.3.2 Slotted Patch Antenna

The introduction of slots on the patch antenna has the effect of reducing its physical size and is commonly used as a miniaturization technique. This effect can be attributed to the apparent increase in length traversed by the surface currents on the antenna. A drawback of this technique is that it results in poorer radiation efficiency and loss in polarisation purity. The latter can be ameliorated by symmetrical positioning of the slots [19].

In this design it is imperative to position the feed such that the symmetry of the slots is maintained relative to its position for the reasons stated. Figures 3.8 and 3.9 highlight these design considerations for linearly polarised patch antennae.

3.4 Design Optimisation

The dimensions of the antenna obtained in Section 3.1 are only a first approximation of the required dimensions since the mathematical models used do not take into account all the factors that come into play when the antenna is excited. To obtain a more realistic set of parameters, these initial values are fed into numerical optimisation algorithms. CST Microwave Studio provides a number of such algorithms of which the Trust Region

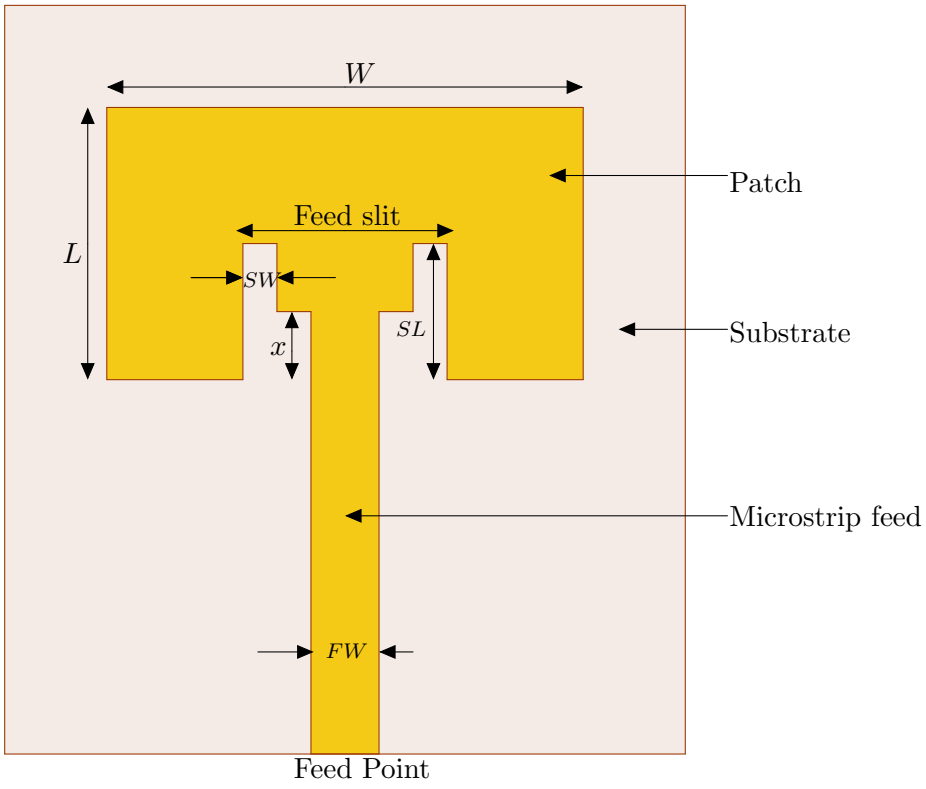

Figure 3.9: Slotted patch with microstrip feed

Table 3.1: 5.2 GHz antennae with FR4 Substrate (h=0.8 mm, $\epsilon_r \approx$ 3.92 (estimate))

Dimensions(mm)	**Std. SMA**	**Slot SMA**	**Std. MS**	**Slot MS**
Length (L)	14.02	13.50	14.44	13.27
Width (W)	19.49	15.79	16.05	15.79
Feed Offset (x)	2.59	3.45	4.30	6.74
Feed Slit (FS)	-	-	3.32	5.00
Feed Width(FW)	-	4.00	1.62	1.62
Slit Width (SW)	-	1.00	-	1.00
Slit Length (SL)	-	9.00	-	9.00

Framework, Nelder Mead Simplex Algorithm and Genetic Algorithm are examples [20].

The Nelder Mead Simplex algorithm was found to converge quickly to the desired goals when supplied with dimensions that were a good approximation to the eventual values. The Trust Region Framework algorithm exhibited a quicker conversion to the desired optimisation goal but required very close estimates to the eventual values as initial input. The genetic algorithm obtained good results but converged too slowly to facilitate rapid prototyping. The latter seems more suited to situations where good estimates of the desired parameters is unknown.

For these designs it was sufficient to provide the bounds for the allowable reflected power or upper bounds on the reflection coefficient S_{11} as goals to be achieved by the numerical optimiser. This provides a result with good matching at the desired resonant frequency and is akin to pulling the desired point on the frequency response curve of the Smith Chart as close as possible to the centre of the chart ($\Gamma = 0$) as shown in Figure 3.10.

A good approach would therefore be to first calculate the approximate dimensions then use these as initial values to the Nelder Mead Simplex algorithm to obtain better estimates. If the matching requirement is very stringent, the output values from this algorithm may be used as inputs to the Trust Region Framework to attain better results. However, this may not always be possible.

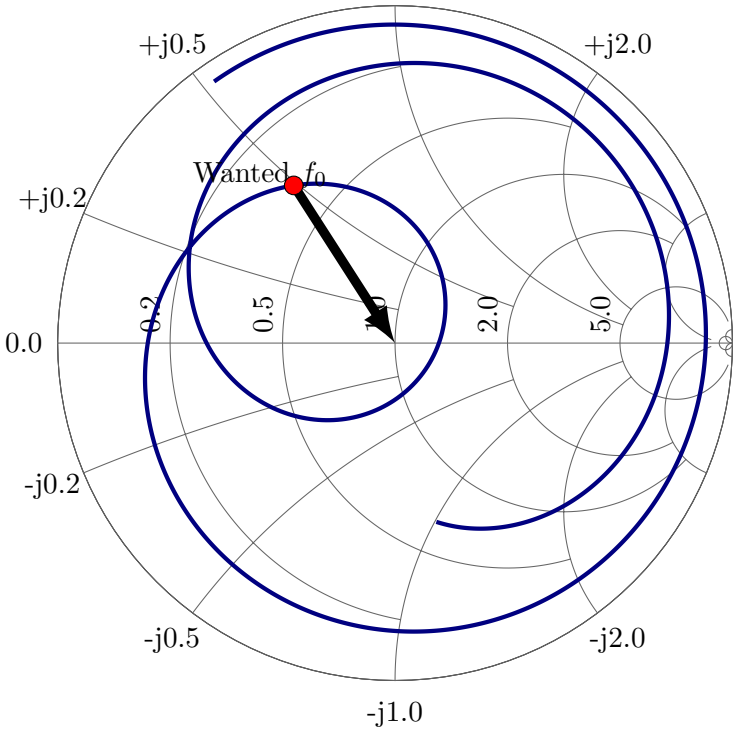

Figure 3.10: S-parameters of the antenna depicted in a Smith Chart. The optimisation goal definition is shown as the black arrow.

Table 3.2: 15 GHz antennae with Rogers™ 3003 Substrate (h=0.5 mm, $\epsilon_r \approx 2.854$ (estimate))

	Dimensions(mm)						
Type	**(L)**	**(W)**	**(x)**	**FS**	**(FW)**	**(SW)**	**(SL)**
Standard	5.729	6.708	1.887	2.317	1.269	-	-
Slotted	5.063	6.322	2.059	3.597	1.269	0.725	2.845

Table 3.3: 28 GHz antennae with Rogers™ 3003 Substrate (h=0.5 mm, $\epsilon_r \approx 2.861$ (estimate))

Dimensions(mm)	**(L)**	**(W)**	**(x)**	**Feed Slit**	**(FW)**
Standard	3.031	3.664	1.121	1.703	1.16

3.5 Manufactured specifications

The antenna dimensions for the standard rectangular patch and the slotted patch are shown in Tables 3.1 and 3.2 for 5.2 GHz and 15 GHz respectively. As is evident from the dimensions, given the same resonant frequency the length and width of the antenna for the slotted case are shorter than those of the standard patch.

At 28GHz, antenna dimensions are sensitive to even the smallest deviations in size. For this reason only the standard patch was designed at this frequency as detailed in table 3.3.

3.6 Approximation of effective dielectric constant and loss tangent

3.6.1 Estimation of FR4 parameters by antenna prototyping

Dielectric substrates, a core component of planar antennae, usually come packaged as Printed Circuit Boards (PCB). The most common of these materials is FR4 whose properties vary widely depending on the PCB manufacturing process and the frequency of use.

It is not always possible to obtain accurate data sheets that adequately capture these properties hence initial designs using such boards may depart greatly from what is depicted by simulations.

FR4 is not particularly suited to high frequency applications given that at such frequencies its losses are considerable. It is therefore common that datasheets for FR4 boards lack dielectric constant and loss tangent values specified at microwave frequencies. A means to establish what these values are at the intended frequencies must be devised before reliably using Computer Aided Design(CAD) tools in designing antennae.

In this instance a prototype antenna was first designed for the given resonant frequency and simulated assuming approximate values of dielectric constant and loss tangent. The prototype was then manufactured and then measured using a Rohde & Schwartz Vector Network Analyser.

Comparisons were then made between the initial simulated results and the measured values noting the disparity between them. Further simulations using a finer mesh were undertaken with varying values of dielectric constant and the mean error between the S_{11} parameters of the simulation and measured results noted.

A subsequent set of designs was undertaken using this new value of dielectric constant and the manufactured antennae measured. A new set of re-simulations with varying values of the loss tangent was undertaken to minimize the phase difference in the impedance response between the measured and simulated results.

The resulting effective dielectric constant and loss tangent values were then determined to be accurate enough to be used as inputs to the simulation models for antennae to be manufactured using these boards. The permittivity value in this case is assumed to be non-dispersive over a narrow band of frequencies and can therefore be characterised as a dielectric constant with a loss tangent.

3.6.2 Estimation of Rogers™ substrate parameters using the quarter wave stub

Antennae for millimeter wave applications require low loss substrates and a dielectric constant that is relatively stable at high frequencies such as teflon. Laminates comprising these substrates are however expensive and in their absence an alternative notably the Rogers™ 3003 laminates have been used in this work for the 15 GHz and 28 GHz frequency range.

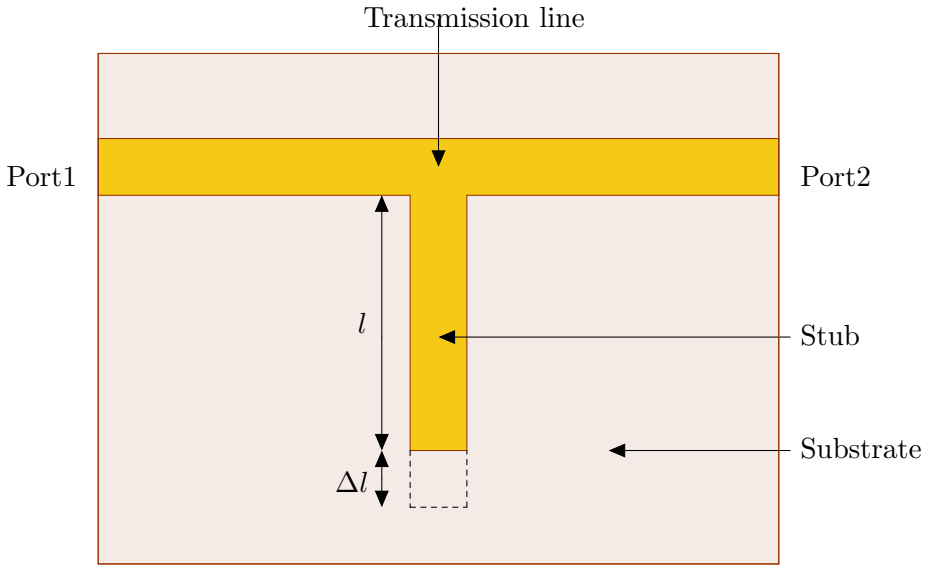

Figure 3.11: Quarter wave stub resonator

Existing datasheets for substrates from the Rogers™ company are for measurements up to 10 GHz. For applications at higher frequencies, it is therefore necessary to determine veritable values of the effective dielectric constant at a given frequency. The quarter wave stub is one such method which has proved useful in this regard [16].

Figure 3.11 shows such a quarter wave resonator that can be used to approximate the effective dielectric constant over a wide frequency range. The transmission parameter S_{21} is measured at the resonant points and the effective dielectric constant calculated as:

$$\epsilon_{\text{eff},n} \approx \left(\frac{nc}{4f_{0,n}(l + \Delta l)} \right)^2, n = 1, 3, 5, ... \tag{3.9}$$

where n is the odd numbered harmonic where resonance occurs, $\epsilon_{\text{eff},n}$ is the effective dielectric constant at the n^{th} resonance, c is speed of light in free space and l is the actual length of the stub, $f_{0,n}$ is the n^{th} resonant frequency and Δl is the effective extra length created by fringing effects at

the open end of the stub given by the empirical formula in [21] as:

$$\Delta l = \left(\frac{\zeta_1 \zeta_3 \zeta_5}{\zeta_4} \right) h \tag{3.10}$$

where

$$\zeta_1 = 0.434907 \left(\frac{K_1 + 0.26}{K_1 - 0.189} \right) \left(\frac{R^{0.8544} + 0.236}{R^{0.8544} + 0.87} \right) \tag{3.11}$$

$$\zeta_2 = 1 + \left(\frac{R^{0.371}}{2.358\epsilon_\mathrm{r} + 1} \right) \tag{3.12}$$

$$\zeta_3 = 1 + \left(\frac{0.5274 \ \tan^{-1}(0.084 R^{1.9413/\zeta_2})}{K_2} \right) \tag{3.13}$$

$$\zeta_4 = 1 + \left[0.0377 \ \tan^{-1}(0.067 R^{1.456}) \right] \left[6 - 5e^{(0.036(1-\epsilon_\mathrm{r}))} \right] \tag{3.14}$$

$$\zeta_5 = 1 - \left[0.218 \ e^{-7.5R} \right] \tag{3.15}$$

$$K_1 = \epsilon_\mathrm{eff}^{0.81} \tag{3.16}$$

$$K_2 = \epsilon_\mathrm{eff}^{0.9236} \tag{3.17}$$

$$R = \frac{W}{h} \tag{3.18}$$

W is the width of the microstrip line, h the thickness of the substrate, ϵ_r is the nominal relative permittivity of the dielectric as shown in Figure 3.2 and ϵ_eff is the effective dielectric constant as given by equation (3.4).

The wavelength, in the substrate, at the first resonant frequency is then calculated as [16]:

$$\lambda_\mathrm{g} = 4 \left\{ l + \Delta l \right\}. \tag{3.19}$$

3.7 Manufacturing process

The antennae designed as mentioned in Sections 3.3 and 3.5 were output as machining files in the Gerber file format [22] common in computer aided manufacturing. These files were input to the LPKF™ ProtoLaser U3 machine[23] to specify which areas on the surface of the laminate the copper film should be extracted. For designs, made for the Rogers™ RO3003 substrate, which required drilling, additional files specifying the position and size of the holes were also supplied. The latter files ensure that laser

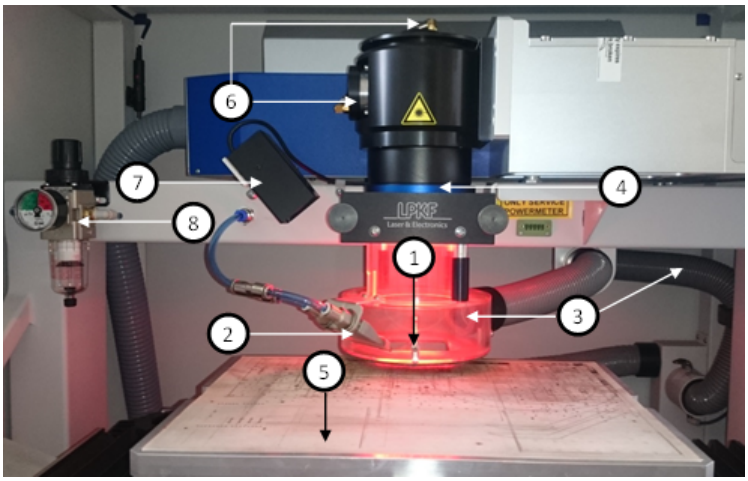

Figure 3.12: LPKF™ ProtoLaser U3 machine
(1)Laser beam operation area, (2)compressed air nozzle, (3)waste suction system, (4)protective screen, (5)working table(vacuum assisted), (6)laser guiding system, (7)camera, (8)pressure gauge

beam cuts through both the substrate and copper laminate.

The detail of the fabrication setup is shown in Figure 3.12. The laser beam heats up the copper in these regions such that it can be blown off by compressed air at high pressures. After each fabrication, it is important to ensure that the screen that protects the lens, shown in Figure 3.13, is cleaned so that the laser beam is not scattered by waste particles in subsequent runs.

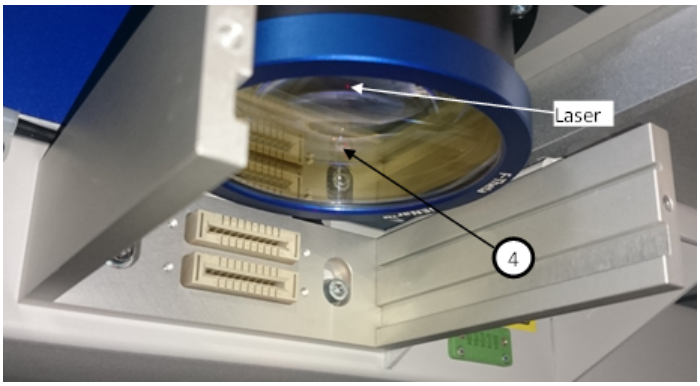

Figure 3.13: Protective screen detail

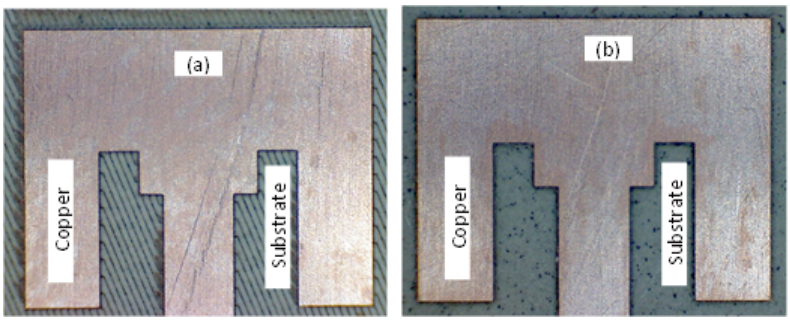

Figure 3.14: Machining detail (a) Diagonal cut (b) Grid cut

Two methods of guiding the laser beam during the copper removal process can be employed: the diagonal cut and the grid cut. In the case of the diagonal cut, the beam is guided to move in a diagonal direction relative to the reference plane. In the grid cut method, the beam first moves in a vertical direction relative to the reference plane and in a second phase moves in a horizontal direction with respect to the reference plane. The resulting output is as shown in Figure 3.14.

Chapter 4

Results

4.1 Measurement Setup

The measurements of antennae resonant at 5.2 GHz were made using a Vector Network Analyser (VNA) with a maximum frequency of 10 GHz. Subsequent measurements of antennae for use at 15 GHz and 28 GHz were made using a precision VNA with a maximum frequency of 67 GHz. The equipment was setup as shown in Figure 4.1. Care was taken to ensure that the Antenna Under Test (AUT) faced directly upwards to minimise the effect of reflections from surrounding objects.

4.2 5.2 GHz Prototypes

4.2.1 Permittivity and loss estimates

The Figure 4.2 shows the measurement results obtained from the prototype antennae designed for PCB boards with a nominal relative permittivity of 4.3. The measured resonant frequency was 5.488 GHz a deviation of almost 6% of the design frequency of 5.2 GHz. Making inference to equation (3.1) this value was observed to be higher than the real permittivity of the actual FR4 substrate.

Using the technique outlined in Section 3.6.1, a closer approximation to the real value of the dielectric constant was obtained as 3.92. Subsequent designs made using this value for permittivity exhibited a deviation of almost 1% from the design frequency of 5.2 GHz as shown in Figure 4.6.

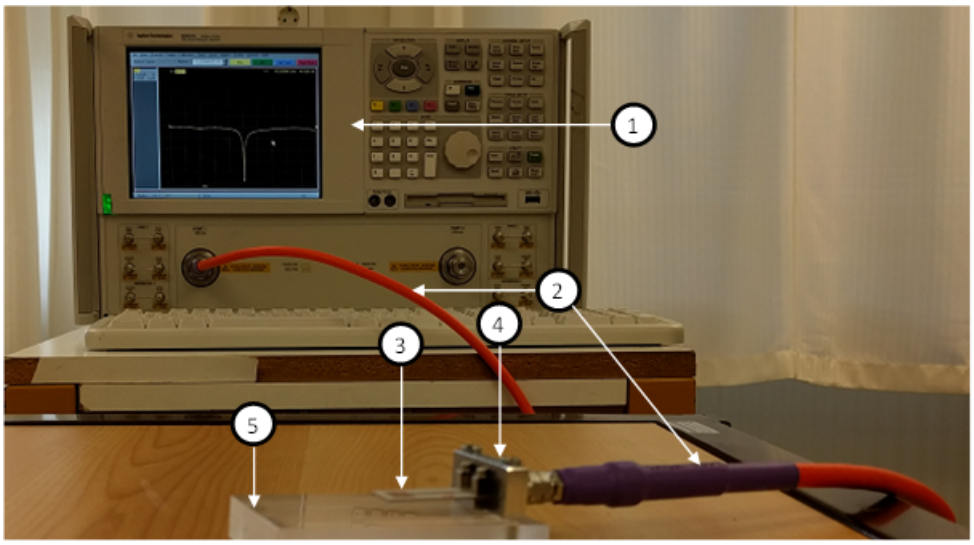

Figure 4.1: Measurement Setup
(1) Vector Network Analyzer (VNA), (2)connector cable, (3)Antenna Under Test (AUT), (4)stabilising bracket, (5)antenna holder

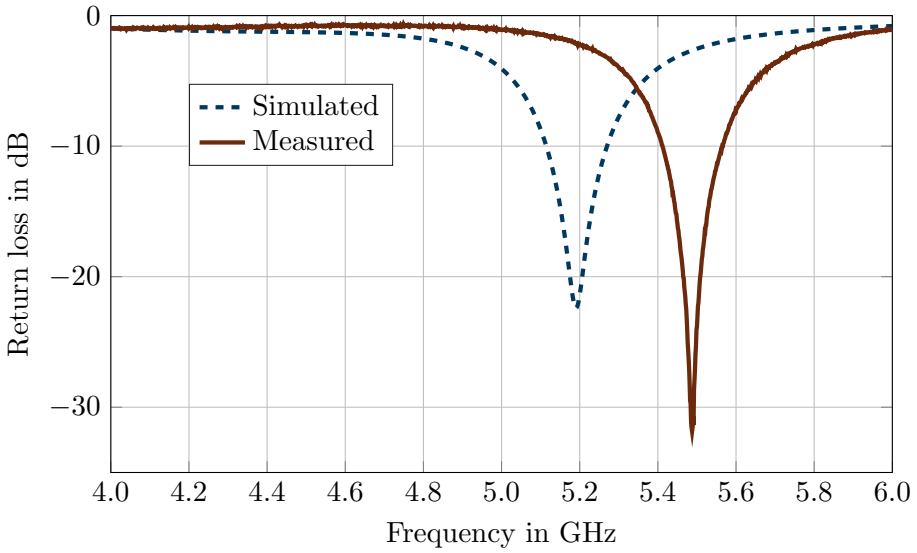

Figure 4.2: FR4 antenna prototype return loss. For simulations the relative permittivity was estimated at $\epsilon_r = 4.3$ and the connector is modeled as a transmission line of length 2.4mm

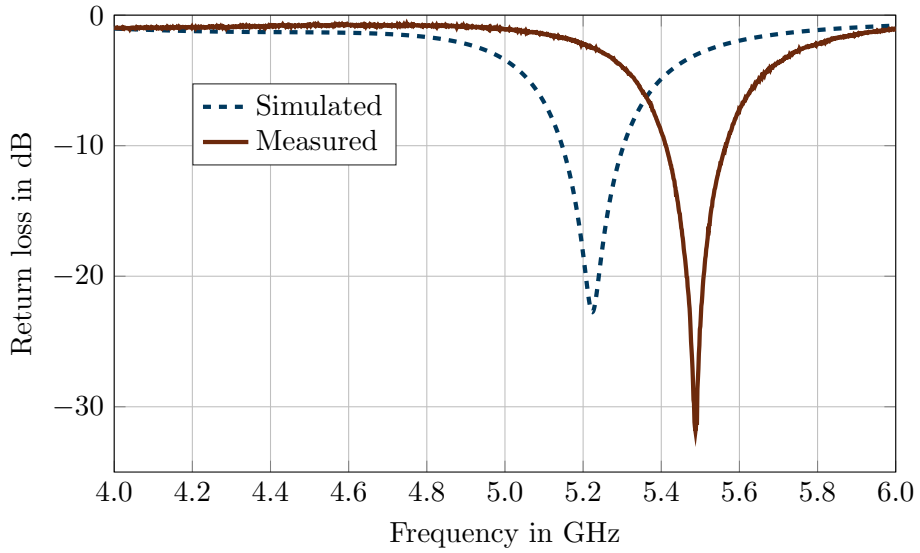

Figure 4.3: FR4 antenna prototype return loss. For simulations the relative permittivity was estimated at $\epsilon_r = 4.3$ and the connector is modeled as a transmission line of length 8.0mm

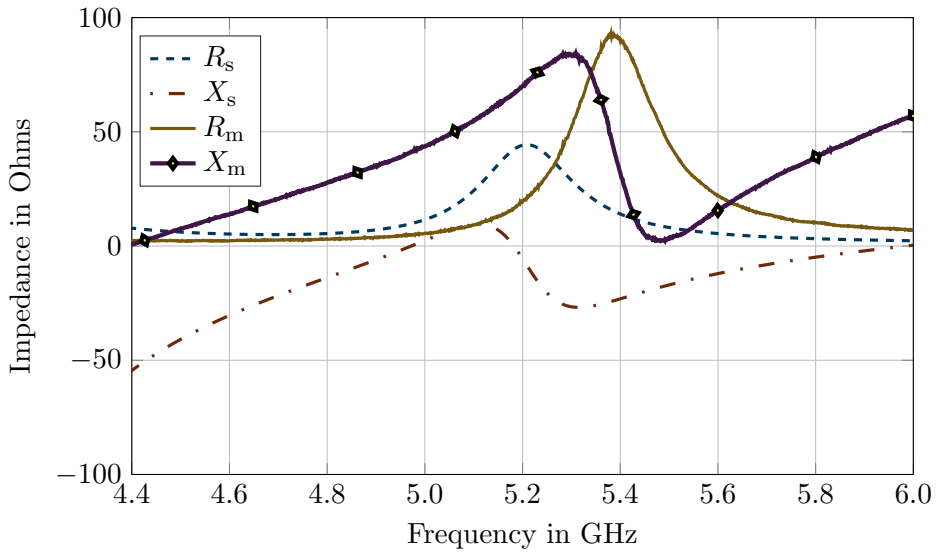

Figure 4.4: FR4 antenna prototype impedance response. For simulations the relative permittivity was estimated at $\epsilon_r = 4.3$ and the connector is modeled as a transmission line of length 2.4mm

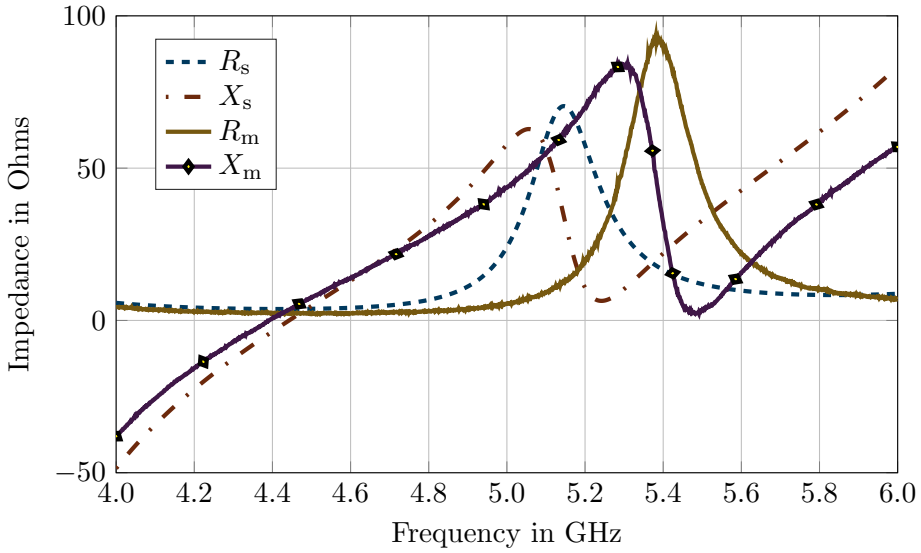

Figure 4.5: FR4 antenna prototype impedance response. For simulations the relative permittivity was estimated at $\epsilon_r = 4.3$ and the connector is modeled as a transmission line of length 8.0mm

The 10 dB fractional bandwidth was measured as 2.8% as compared to 3.4% of the initial simulated designs. The main reason for this is that the loss term of the permittivity was not taken into account when estimating the dielectric constant. The fractional bandwidth increases with an increase in loss tangent. From equation (1.5) this may be explained by a reduction in stored energy, hence lower Q, as more energy is lost.

The value of 0.025 for the initial simulations was higher than the real loss tangent. A closer match to the real value was found to be 0.015 as shown in Figure 4.6. This results in a fractional bandwidth of 2.77 which was comparable to the measured value.

The correct modelling of the length of the SMA feed was seen to have little effect on the frequency of resonance. Its main effect was on the absolute value of the return loss as well a the phase response of the antenna as shown in Figures 4.2 - 4.8.

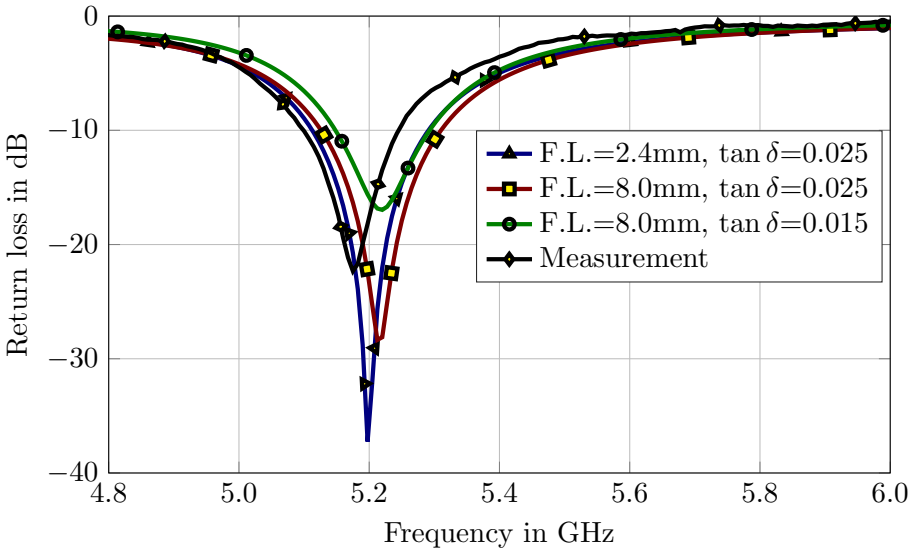

Figure 4.6: Comparison of return loss. For simulations the relative permittivity was estimated at $\epsilon_r = 3.92$
F.L.=Feed Length, $\tan\delta$=loss tangent

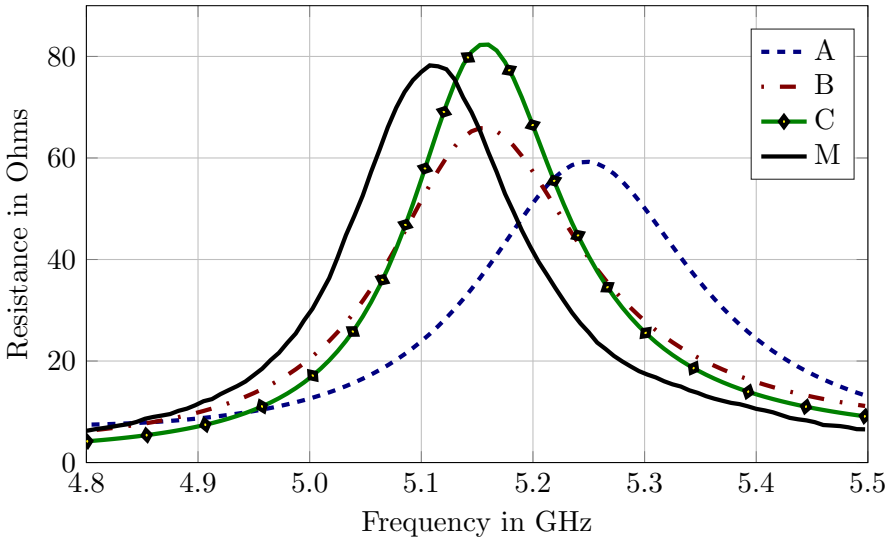

Figure 4.7: Comparison of resistance values about resonance
A (F.L.=2.4mm, $\tan\delta$=0.025), B (F.L.=8.0mm, $\tan\delta$=0.025),
C (F.L.=8.0mm, $\tan\delta$=0.015), M (Measurement)

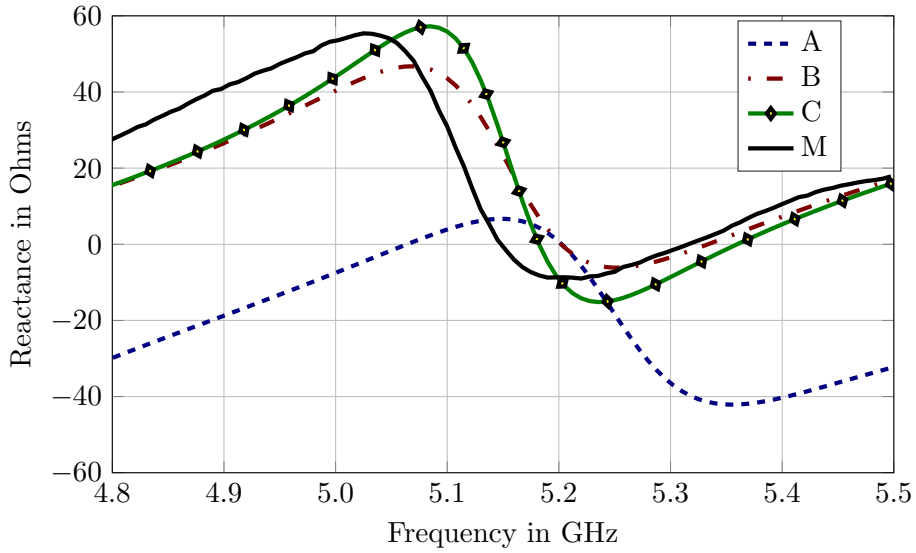

Figure 4.8: Comparison of reactance values about resonance
A (F.L.=2.4mm, $\tan\delta$=0.025), B (F.L.=8.0mm, $\tan\delta$=0.025),
C (F.L.=8.0mm, $\tan\delta$=0.015), M (Measurement)

4.2.2 Relative performance

The proximity of the feed to the patch was found to influence the resonant frequency as shown in Figure 4.9. The direct SMA feeds showed a marked disparity in the position of the resonant frequency as compared to the microstrip feeds. The influence of the connector and the excitation cable on the performance of the antenna may be likely causes of this. In contrast the antennae excited using microstrip feed lines exhibited very slight variations with respect to each other.

4.3 15 GHz Prototypes

4.3.1 Permittivity and loss estimates

Antennae for operation at 15 GHz and 28 GHz were manufactured using Rogers™ 3003 substrate whose characteristics, as detailed in the datasheets, are measured at 10 GHz. In order to obtain better estimates of the permittivity at these frequencies, a quarter wave stub was used as described in Section 3.6.2.

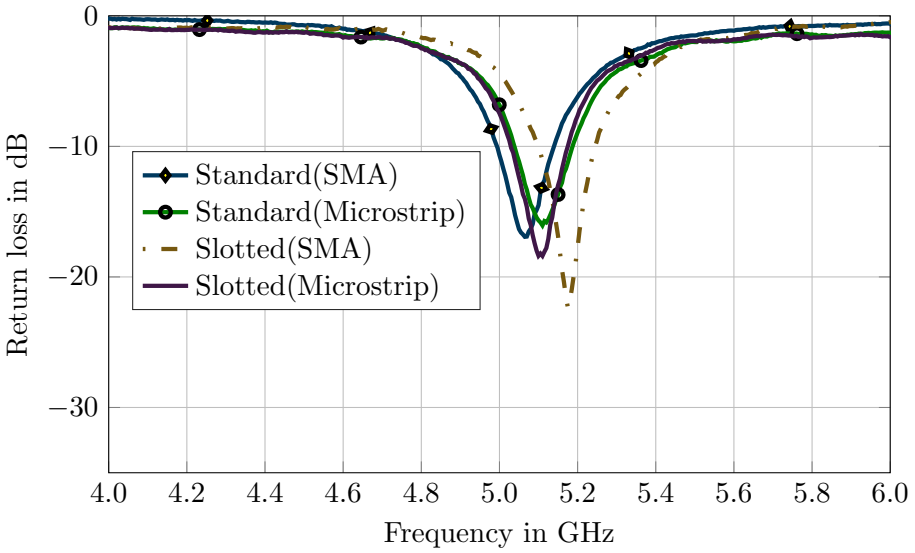

Figure 4.9: Comparative Return loss performance

Figure 4.10 shows the measurement results from 2 similar stubs and the subsequent fitting simulations run to obtain the value of the relative permittivity at the resonant frequencies. The resulting relative permittivity values were used in a regression model as shown in Figure 4.11 to obtain an estimate for the 28 GHz range.

4.3.2 Antenna performance

Two different designs were investigated at this frequency: the standard patch and the slotted patch. Further the two methods for guiding the laser beam in removing the copper from the laminate described in Section 3.7 were also investigated.

The grid technique has the disadvantage of producing more waste material. The resulting waste material fouls the lens screen resulting in imprecise copper removal. The diagonal cut is found to be more consistent compared to the grid cut as shown in Figures 4.12 and 4.13.

It was also observed that the more intricate the design, the greater the deviation from the resonant frequency as shown in Figure 4.13. This can be attributed to the cumulative errors in the many different dimension

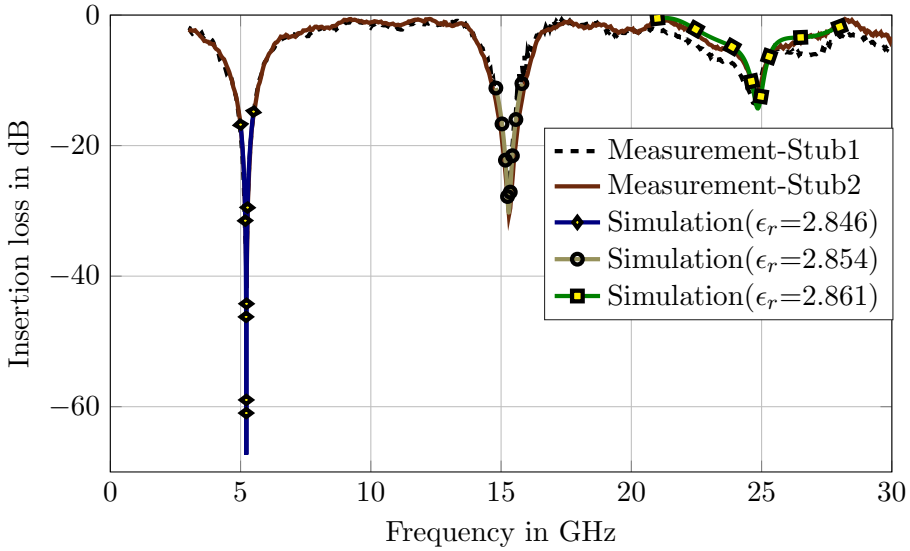

Figure 4.10: Insertion loss characteristic of quarter wave stub

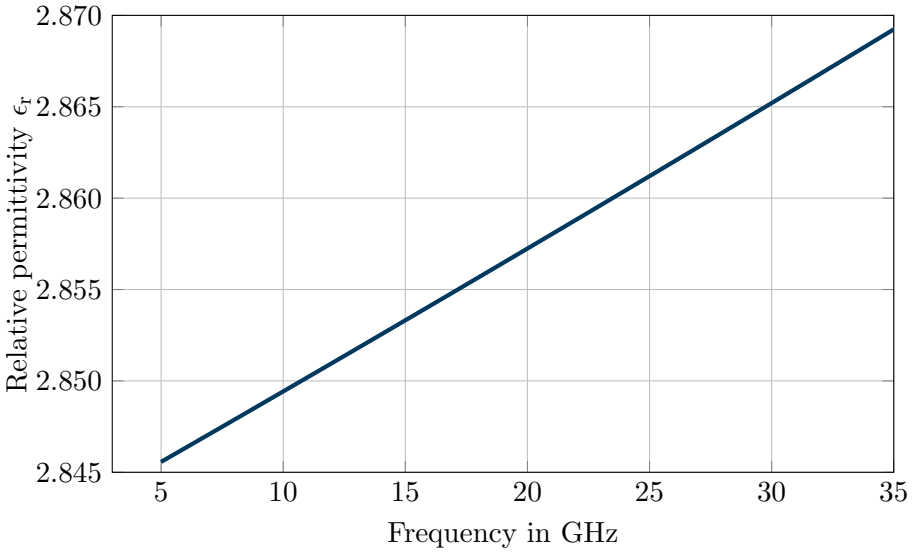

Figure 4.11: Relative permittivity estimate of Rogers™ 3003 substrate

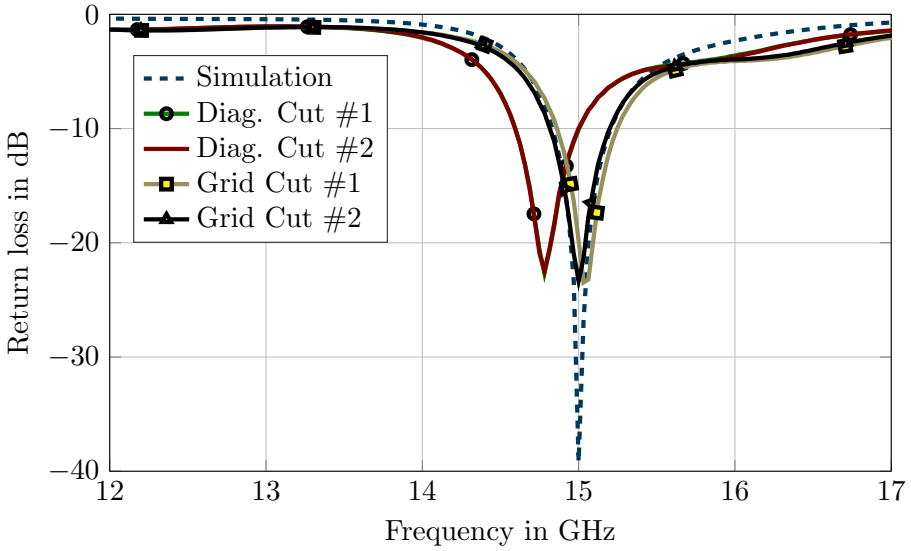

Figure 4.12: Return loss response of standard antennae

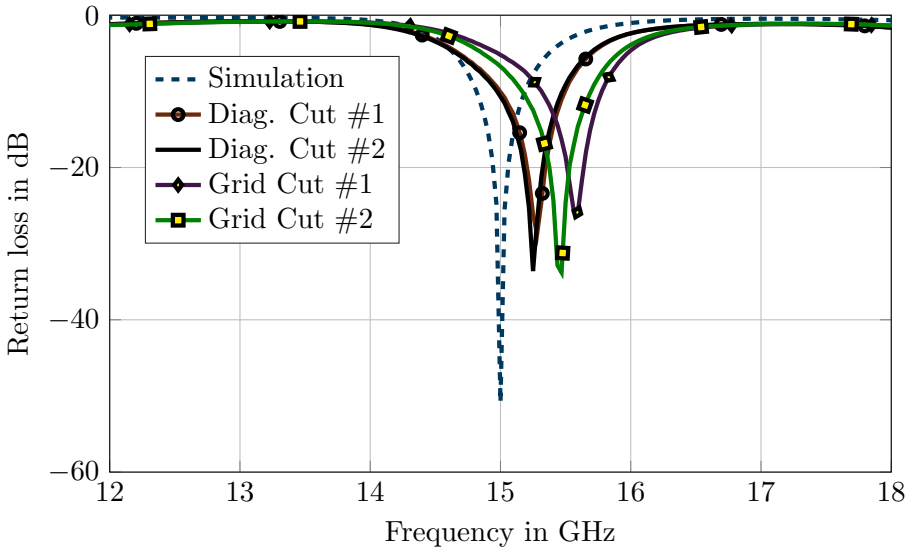

Figure 4.13: Return loss response of slotted antennae

Table 4.1: Approximate % deviation from design for standard antennae at 15 GHz

Laser Cut \Dimension	L	W	x	Feed Slit
Grid	0.51	0.79	0.05	2.33
Diagonal	0.37	0.66	0.05	1.77

Table 4.2: Approximate % deviation from design for slotted antennae at 15 GHz

Laser Cut \Dimension	L	W	x	Feed Slit	SW	SL
Grid	0.30	1.01	0.97	1.92	4.55	0.67
Diagonal	0.63	0.89	0.58	1.56	4.00	0.53

specifications. The diagonal cut in this case results in a deviation of about 1.5% from the resonant frequency and the grid cut results in a maximum deviation of 3.5% from the resonant frequency.

The slotted patch design however results in a fractional bandwidth of 3.4% compared to 2.5% for the standard patch as depicted in Figure 4.14. A likely cause is that this design results in less energy storage in the radiating structure hence a lower Q factor resulting in an increase of bandwidth as specified by equation (1.5).

4.4 28 GHz Prototypes

At this frequency, the antenna's S_{11} response was found to deviate slightly from the sharp narrowband characteristic evident at 5.2 GHz and 15 GHz as shown in Figure 4.15.

The 10 dB bandwidth of the antennae fabricated using the diagonal cut was found to be nearly 1.8 GHz and those fabricated using the grid cut were found to have a bandwidth of about 1.9 GHz. The simulated band-

Table 4.3: Approximate % deviation from design for standard antennae at 28 GHz

Laser Cut \Dimension	L	W	x	Feed Slit
Grid	0.03	0.57	0.36	2.64
Diagonal	0.20	0.57	0.36	2.11

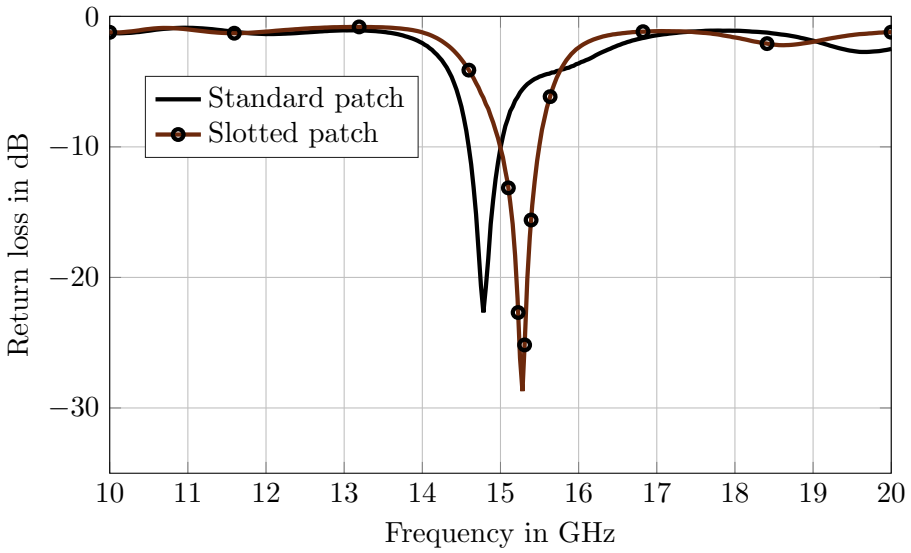

Figure 4.14: Comparison of Standard and Slotted antenna responses

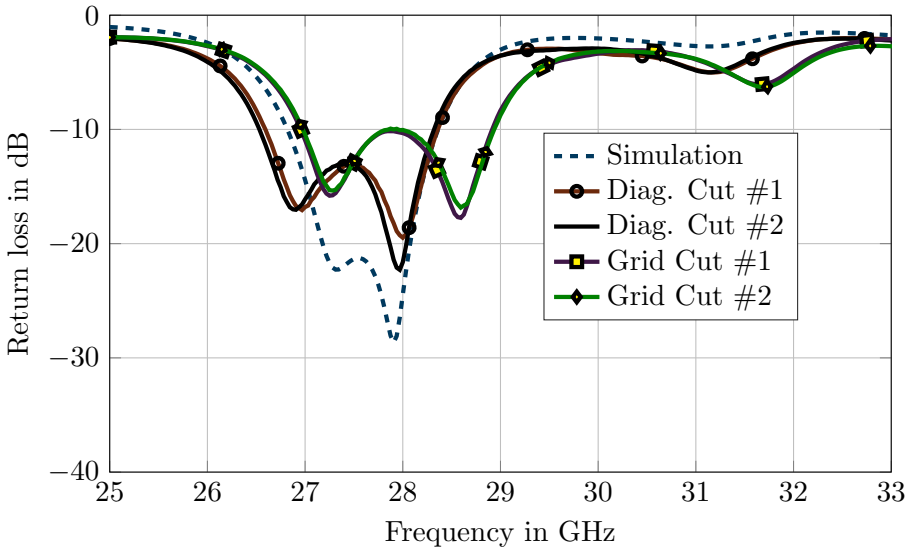

Figure 4.15: Return loss response of the standard antenna

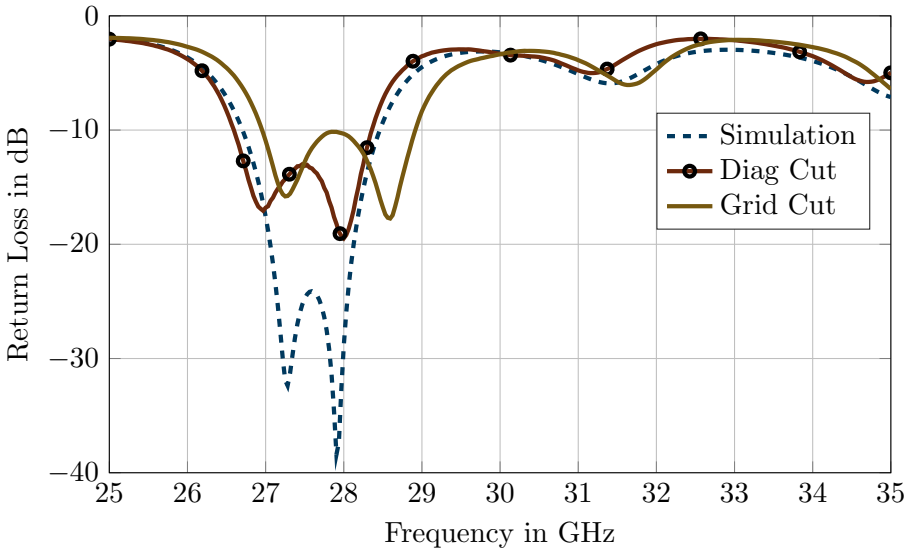

Figure 4.16: Comparison of antenna responses. Simulation with higher loss tangent.

width was found to be about 15% less than the measured values. This was indicative of an increase in the loss term of the permitivitty which was not characterised in the estimation of the dielectric constant. The nominal value of 0.001 indicated in the datasheet for the RO3003™ substrate was found to be rather low. Re-simulation with a loss tangent of 0.01 gave the response shown in Figure 4.16 with a bandwidth of 1.8 GHz which was comparable to the measured values. The loss in the substrate at these frequencies was seen to exhibit a large deviation from the datasheet values measured at 10 GHz.

Chapter 5

Conclusion

5.1 Summary

This work has investigated the design considerations required to design, fabricate and test high performance linearly polarised planar antennae at 5.2 GHz, 15 GHz and 28 GHz using the LPKF™Protolaser U3 machine.

Deviations from the simulated designs were found to be more influenced by the characterisation of the dielectric substrates in the simulation software than by errors in fabrication. The relative permittivity estimation was of particular importance in determining the antenna resonant frequency. At 5.2 GHz, significant deviations were observed for FR4 substrates whose dielectric constant was not accurately characterised.

The sharp frequency response of the reflection coefficient at 5 GHz was found to be a simple yet effective means to determine the dielectric constant when the substrate's relative permittivity is approximately known.

At the relatively higher frequencies of 15 GHz and 28 GHz, the use of a quarter wave stub on a microstrip transmission line was found to be a good means to approximate the dielectric constant. In this case, a two port measurement of the transmission coefficient (S_{21}) and minima fitting simulations varying the dielectric constant at the different resonant frequencies was used.

The value of the dielectric constant in FR4 was found to be highly variant with frequency rendering it unsuitable for high frequency applications. The dielectric constant of the RO3003™ substrate was found to vary slightly with

frequency up to 30 GHz. However the loss tangent was found to increase markedly higher than that indicated in the datasheet at this frequency.

The introduction of slots in the patch antennae was found to improve the fractional bandwidth slightly but also increased the deviation from the expected design response owing to cumulative fabrication errors arising from the intricate design. Fabrication errors were seen to increase when the design had small regions of alternating substrate and conductor.

The diagonal and grid cut techniques for guiding the laser in the copper removal process from the laminate were also investigated. The grid cut method was found to require more frequent cleaning of the equipment between fabrication runs as it produced more waste material.

The responses of antennae produced was also found to be dependent on the technique used. The disparity between antennae produced using the two methods was seen to increase with the frequency of operation.

Manufactured antennae were found to be fairly consistent pointing to high precision of the prototyping machine. However this was not fully tested owing to limitations in time and measurement resources required to determine the actual dimensions of the fabricated antennae.

5.2 Future Work

The statistical accuracy of the prototyping machine needs to be investigated further to determine the appropriate level of confidence the antenna designer can have to ensure that the simulated designs match the real world antennae fabricated.

Given the influence of the loss tangent in the bandwidth response of the antenna, simple techniques to approximate this parameter may need to be explored particularly at high frequencies where losses are more significant.

The effect of the furrows around the edges of the patch antenna arising from the laser cut may also be of interest. This could influence how the antenna radiates given the slight air gap created.

Bibliography

[1] D. Pozar, *Microwave Engineering*. Wiley, 2005.

[2] A. D. Yaghjian and S. R. Best, "Impedance, bandwidth, and Q of antennas," *IEEE Transactions on Antennas and Propagation*, vol. 53, no. 4, pp. 1298–1324, April 2005.

[3] K. Carver and J. Mink, "Microstrip antenna technology," *IEEE Transactions on Antennas and Propagation*, vol. 29, no. 1, pp. 2–24, Jan 1981.

[4] K. Wong, *Planar Antennas for Wireless Communications*, ser. Wiley Series in Microwave and Optical Engineering. Wiley, 2003.

[5] G. A. E. Vandenbosch, "State-of-the-Art in Antenna Software Benchmarking: "Are We There Yet"? [EurAAP Corner]," *IEEE Antennas and Propagation Magazine*, vol. 56, no. 4, pp. 300–308, Aug 2014.

[6] J. Maxwell, *A Treatise on Electricity and Magnetism*. Dover, N.Y., 1954.

[7] T. Rylander, P. Ingelström, and A. Bondeson, *Computational Electromagnetics*, ser. Texts in Applied Mathematics. Springer New York, 2012.

[8] G. A. E. Vandenbosch, "Computational Electromagnetics: Commercial State-of-the-Art and Scientific Roadmaps [EurAAP Corner]," *IEEE Antennas and Propagation Magazine*, vol. 54, no. 2, pp. 283–288, April 2012.

[9] A. Vasylchenko, Y. Schols, W. D. Raedt, and G. A. E. Vandenbosch, "Quality Assessment of Computational Techniques and Software Tools for Planar-Antenna Analysis," *IEEE Antennas and Propagation Magazine*, vol. 51, no. 1, pp. 23–38, Feb 2009.

[10] J. Van Bladel, *Electromagnetic Fields*, ser. IEEE Press Series on Electromagnetic Wave Theory. John Wiley & Sons, 2007.

[11] A. R. Djordjevic, R. M. Biljie, V. D. Likar-Smiljanic, and T. K. Sarkar, "Wideband frequency-domain characterization of FR-4 and time-domain causality," *IEEE Transactions on Electromagnetic Compatibility*, vol. 43, no. 4, pp. 662–667, Nov 2001.

[12] A. E. Engin, "Extraction of Dielectric Constant and Loss Tangent Using New Rapid Plane Solver and Analytical Debye Modeling for Printed Circuit Boards," *IEEE Transactions on Microwave Theory and Techniques*, vol. 58, no. 1, pp. 211–219, Jan 2010.

[13] S. J. Orfanidis, *Electromagnetic waves and antennas*. Rutgers University New Brunswick, NJ, 2002.

[14] I. J. Bahl and D. K. Trivedi, "A Designer's Guide to Microstrip Line," *Microwaves*, pp. 174–182, May 1977.

[15] "Microstrip line calculator," http://www.microwaves101.com/encyclopedias/microstrip-calculator, accessed: 2016-04-20.

[16] J. Carroll, M. Li, and K. Chang, "New technique to measure transmission line attenuation," *IEEE Transactions on Microwave Theory and Techniques*, vol. 43, no. 1, pp. 219–222, Jan 1995.

[17] "SouthWest Microwave^{TM}," http://mpd.southwestmicrowave.com/, accessed: 2016-06-15.

[18] S. M. Inc., "Optimizing Test Boards for 50 GHz End Launch Connectors Grounded Coplanar Launches and Through Lines on 30 mil Rogers 4350 with Comparision to Microstrip," http://mpd.southwestmicrowave.com/showImage.php?image=439, accessed: 2016-04-24.

[19] M. U. Khan, M. S. Sharawi, and R. Mittra, "Microstrip patch antenna miniaturisation techniques: a review," *IET Microwaves, Antennas Propagation*, vol. 9, no. 9, pp. 913–922, 2015.

[20] C. V. Sokol, "Optimization techniques in CST Studio Suite." in *EUGM 2011*, 2011.

[21] M. Kirschning, R. H. Jansen, and N. H. L. Koster, "Accurate model for open end effect of microstrip lines," *Electronics Letters*, vol. 17, no. 3, pp. 123–125, February 1981.

[22] "Gerber File Format Specification," https://www.ucamco.com/files/downloads/file/81/the_gerber_file_format_specification.pdf?ac40b80482e8e1864842659f85fb1c9c, accessed: 2016-04-30.

[23] "LPKF ProtoLaser U3," http://www.lpkf.com/products/rapid-pcb-prototyping/laser-circuit-structuring/laser-micromaterial-processing.htm, accessed: 2016-04-30.

[24] "Inkscape®," https://inkscape.org/en/, accessed: 2016-05-21.

Appendix A

Optical Microscope Measurements

The measurements to determine the deviations from the design in the physical dimensions were made with the help of an optical microscope and calibration kit as shown in Figure A.1. The calibration kit was placed under the microscope and its zoom adjusted until the correct focus was attained. An image of this was then acquired. With the settings maintained, the different types of antennae were then photographed and the resulting images saved.

Inkscape® [24] software was then used to trace the outlines of the images into a vector representation. The resulting images could then be expanded without losing resolution. The calibration reference was obtained by determining the number of pixels taken to measure 5 mm as shown in A.1. The antennae dimensions were then measured in terms of pixels and converted to mm using the reference measurement. The results obtained are as shown in Tables A.1 - A.3.

Table A.1: Measurements of standard antennae at 15 GHz

Cut \Dimension	**L**	**W**	**x**	**Feed Slit**
Grid	5.758	6.761	1.888	2.371
Diagonal	5.750	6.752	1.888	2.358

Table A.2: Measurements of slotted antennae at 15 GHz

Cut\Dimension	**L**	**W**	**x**	**Feed Slit**	**SW**	**SL**
Grid	5.078	6.386	2.079	3.666	0.758	2.864
Diagonal	5.095	6.378	2.071	3.653	0.754	2.860

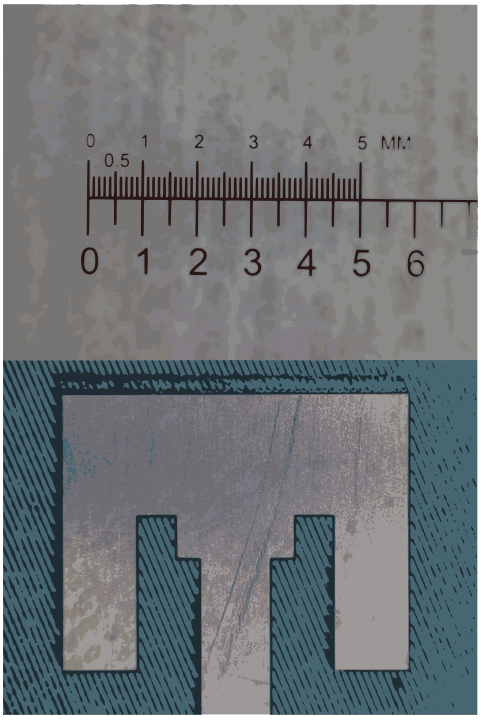

Figure A.1: Vectorised images for measurement of antennae

Table A.3: Measurements of standard antennae at 28 GHz

Cut \Dimension(mm)	**L**	**W**	**x**	**Feed Slit**
Grid	3.03	3.684	1,125	1.748
Diagonal	3.025	3.684	1.125	1.739

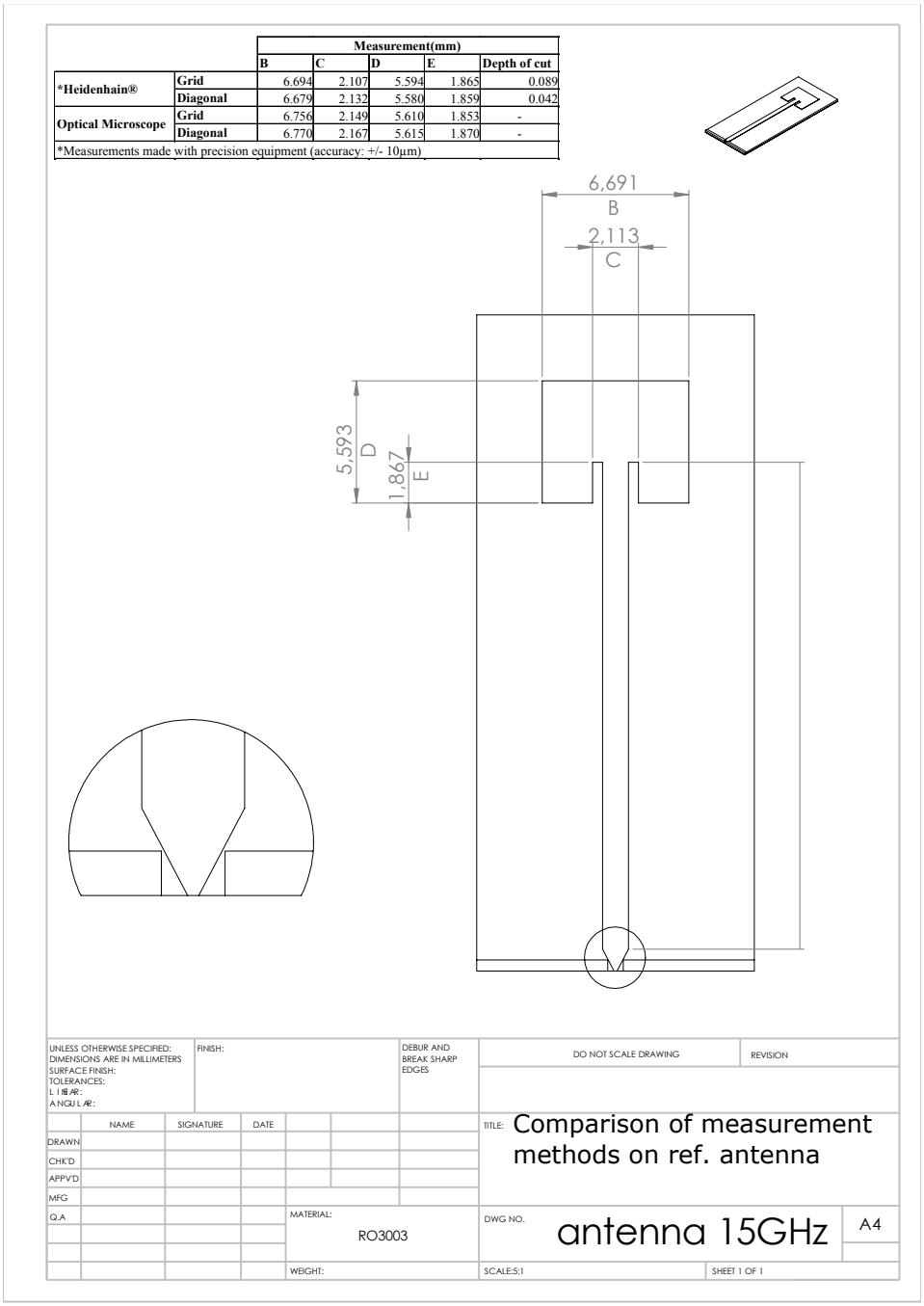

Figure A.2: Comparative reference measurement

LUND
UNIVERSITY

Series of Master's theses
Department of Electrical and Information Technology
LU/LTH-EIT 2016-515

http://www.eit.lth.se